The onset of churn flow in vertical tubes : effects of temperature and tube radius

THE ONSET OF CHURN FLOW IN VERTICAL TUBES

- Effects of temperature and tube radius -

C.W.M. van der Geld

Report WOP-WET 85.010

T A B L E O F C O N T E N T

ABSTRACT

In this paper criteria for the onset of churn flow in vertical tubes are derived theoretically. The hypothesis is investigated, that plug-churn flow pattern transition in vertical tubes is caused by film instability governed by nonlinear, dispersive interaction with the flow in a gas/vapor pocket or plug, in which circulation is present. A core velocity distribution is derived that can represent this internal circulation.

There is no attempt to study wave development explicitly. The instantaneous rate of amplitude dispersion, or "shearing", is accounted for in the stability calculations. It is shown that instability only occurs if the wave amplitude is that large, that strong internal gas/vapor motions can effectively affect the wave.

Results of stability calculations and theoretical criteria for the onset of churn flow are presented, including dependencies on tube radius and temperature. A calculation procedure is presented for the determination of the flow pattern present with the aid of the criteria derived. Resulting predictions are compared with experimental data, some of which are new and obtained with an objective instrument, the so-called Flow Pattern Indicator. The theory is shown to be compatible with observed entry length phenomena.

This study was supported by the Netherlands Organization for the Advancement of Pure Research (Z.W.O.).

0 INTRODUCTION

Gas-liquid and vapor-liquid flows have a manifold occurrence in the chemical and oil industry. For given flows of two phases in a given channel certain classes of interfacial distributions can be delineated. They are commonly called flow regimes or flow patterns. The study of boiling liquids is important in the context of safety in power plants for instance. The transition from annular to mist flow corresponds to "dry-out" or "burn-out" of a tube, and determines operating limits of cooling systems.
The understanding and delineation of flow patterns are particularly important in practical design, when more accurate results are needed. The nature of the physical interactions causing flow pattern transitions varies from one transition to an other. In this paper attention is focussed on plug-churn flow pattern transition in vertical tubes. Theoretical criteria for the onset of churn flow in gas-liquid systems as well as for water-vapor flows of any temperature will be derived. A calculation procedure will be put forward to predict the flow pattern present with the aid of the criteria derived. Effects of temperature, tube radius and mass density will be studied. Entry length theories will be shown to be complementary to the stability theory to be presented. In chapter one, underlying physical assumptions and experimental observations will be discussed.

In plug flow or slug flow large, characteristically bullet-shaped bubbles are separated by regions containing dispersions of small bubbles. Around each rising Taylor bubble, or more simply "plug", an annular liquid film flows downward. See figure 1. The main assertion in this paper is that, when this film is unstable, in a sense to be further specified, plug flow can not be present, and another flow regime occurs. When bubble flow, an agglomeration of gas/vapor pockets with diameters less than a quarter of the tube radius, is out of the question the other regime is churn flow (Hetsroni, 1982). Semi-churn (Van der Geld, 1984) and semi-annular flow (Haberstroh and Griffith, 1969) are other names that have been introduced for churn flow. The names point out different features of the regime and global resemblances to other flow patterns.
Experimental and physical observations support the idea that plug-churn flow pattern transition is caused by film instability governed by a non-linear

interaction. D. Nicklin and J. Davidson (1962) have tried to relate a linear stability analysis to the transition from plug flow to churn flow, but one of the things that will be argued in this paper is that a linear analysis is inappropriate to describe this transition.

A lead to a precise characterization of churn flow is given by measurements made with high speed cinematography and the Flow Pattern Indicator (see Van der Geld, 1984). These measurements reveal a resemblance between plug flow and churn flow. Because of fast movements and an oscillatory behaviour of the two-phase flow, this resemblance is obscure for the naked eye. The objective measurements delineate churn flow as an intermittent type of flow with remnants of liquid bridgings and with a water film with much air entrapped in it.
In the published literature there is virtually no mention of the occurrence of foamy lumps in churn flow. An exception is represented by Fernandes (1981), who calls them "lumping phenomenons". Consequent practical implication is the fact, that the resemblance between plug flow and churn flow has escaped attention. This constitutes a serious gap in the description of plug-churn flow pattern transition in vertical multiphase flows. Hithertoo, resemblances between plug and churn flow have been mentioned only by Fernandes (1981) and Van der Geld (1984).
The occurrence of highly turbulent and bubbly liquid bridgings in churn flow is a result of the fact that at some locations a steady stream is slowed down considerably until it (almost) alters direction. The required energy loss at these lumps is partly achieved by energy fluxes in waves and by viscous and turbulent dissipation, but mostly by an intense foaming.

It is a little hard to describe the exact nature of churn flow comprehensively. A definition by means of photographs has been given by Van der Geld (1984) for example. Based on observations, churn flow can be formally defined as a flow in which at every instant in a volume made up of cross-sections of the tube each phase occupies non-trivial scattered sub-volumes that are multiple connected. The definition separates churn flow from bubble flow because bubble flow is multiple connected only for the liquid phase, and from bubbly annular flow with droplets because this flow is not scattered since a restriction to the core yields mist flow, and the

vapor part of mist flow is not multiple connected. Scattered means that the convex closure of the volume of observation can not be restricted to a non-trivial convex subvolume of the same axial length without changing the other features of the flow as described in the definition.

1 GENERAL CONSIDERATIONS

1.1 Physical considerations

1.1.1 Experimental observations. The appearance of foam on a water film is caused by the entrapping of air. Observations indicate that this additional mode of energy dissipation is typical for liquid films in churn flow. A breakdown of the integrity of the water surface has occurred, which gives support to the assumption that the onset of churn flow is related to the point where film instability occurs. This observation also gives a first hint regarding the kind of waves involved in the transition from plug to churn flow. The presence of large amplitude waves in churn flow and plug flows close to transition to churn flow, is inferred from photographs and indicated by the appearance of foaming. Periodic gravity waves on deep water are known (Longuet-Higgins, 1975) to have a maximum energy flux relative to the crests corresponding to a certain amplitude. Waves with still larger amplitudes exhibit foaming in order to dissipate the excess energy. Quantitative results for gravity waves on deep water are of limited value to us, because only flow regimes in (nearly) vertical tubes are considered in this paper and moreover the waves under consideration appear on a strong current. Only a maximum value of 0.74 for $k\eta$ is noted, where k represents the wave number and η the elevation above the undisturbed water level.
An other reason to expect large amplitude waves to be involved in the transition from plug to churn flow, which shall be named the P-C transition henceforth, is associated with the circulation that is present in the plug core (see Filla, Davidson, Bates and Eccles, 1976, for example). The circulation is the result of the drag exerted by the falling liquid film and of the upward motion of the plug as a whole. Like in some freely moving bubbles, toroidal vortices are formed in the gas region. In this way the core flow is closely connected with the film flow. Obviously, in these circumstances one cannot expect instability of waves at the interface to occur in the same way as in the usual Helmholtz theory. On the contrary, it will be argued that large, wavy disturbances occur on the liquid film of plugs close to transition to churn flow anyhow, and that these disturbances become unstable because of the interaction with core motions. It will be demonstrated, that for a given set of averaged or superficial velocities,

instability only occurs when the wave amplitude is that large, that it can be affected by internal vapor motions having sufficiently large velocities relative to the water. In figure 4 this is clearly indicated, since the stability factor √FACT increases with increasing wave stability. In the limit for $\eta \to 0$ the liquid flow is found to be always stable, as can be shown from the starting equations or, more conveniently, from the results (59) and (64) in sections 2.3 and 2.4.

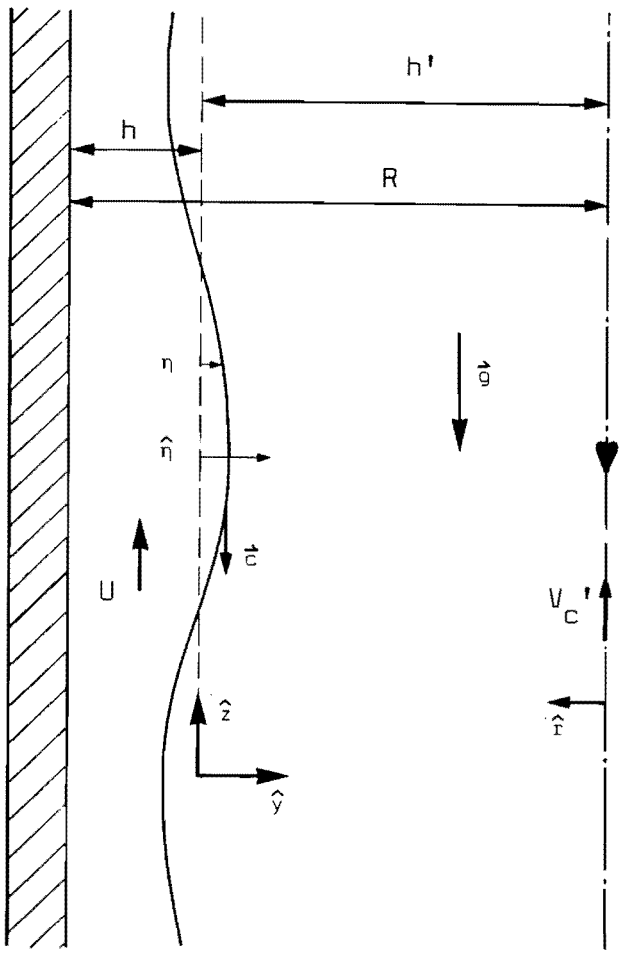

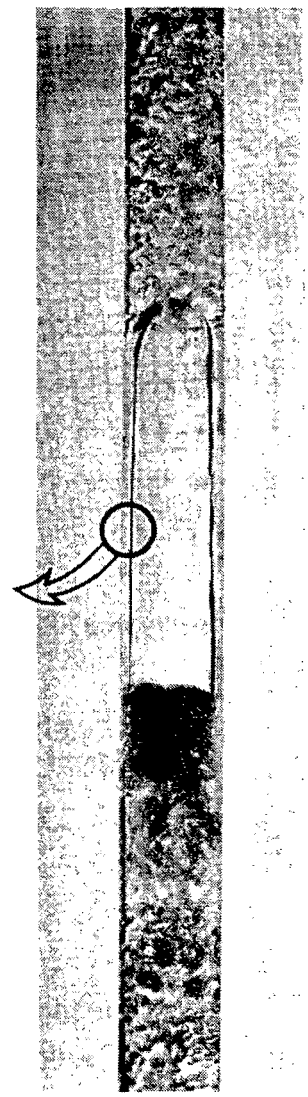

Figure 1
Coordinate systems

Another reason to expect waves with large amplitude is the fact that in the water film of a plug, bubbles frequently appear. See figure 1. These bubbles move radially inward, i.e. towards the interface, due to an interplay between the buoyance force and the (weak) rotational part of the

(undisturbed) main stream. The bubbles cause large disturbances where they appear near the interface. Eventually they even may explode, losing their content in the gas/vapor core. This provides a strong background noise, from which modulations may develop in the sense to be discussed in 1.1.2. Moreover, like all moving objects bubbles rising relative to the main stream are the direct cause of surface waves; these waves are connected to the wavedrag the bubbles experience.

1.1.2 Origins of large amplitude waves. Waves originating from the nose of the plug grow, which is a reason to expect waves of larger rather than moderate amplitudes. In order to see this and to estimate the growth rate some appropriate equations will now be derived using the variational approach developed by Whitham (1974). For ease of reference the main points of this approach will be very briefly introduced.

Whithams treatment of non-linear dispersed waves is valid in a non-uniform environment with parameters such as the mean liquid layer thickness h sufficiently gradually varying on a scale of wavelengths. The latter restriction is expected to hold approximately near the nose of a plug. The treatment starts from a local phase α, defined such that it increases smoothly by 2π between two successive crests. The phase density k and the phase flow rate $\omega = kc$ then follow from:

$$k = \frac{\partial \alpha}{\partial x} \quad \text{and} \quad \omega = -\frac{\partial \alpha}{\partial t} \quad \text{, whence}$$

$$\frac{\partial k}{\partial t} + \frac{\partial \omega}{\partial x} = 0.$$

Evidently the functional form for α replaces the Fourier analysis description. After introduction of a suitable Lagrangian in terms of a velocity potential φ such as:

$$-\varrho \int_{-h}^{\eta} \left(\frac{\partial \varphi}{\partial t} + \frac{1}{2} (\nabla \varphi)^2 + gz\right) dz$$

derived for waves on shallow water by Luke (1967), and the corresponding Lagrangian density ζ, which is the Lagrangian averaged over a wavelength, Hamilton's principle is used to derive conservation

equations for an appropriate set of parameters. One of them expresses the conservation of wave action $\frac{\partial \zeta}{\partial \omega}$:

$$\frac{\partial}{\partial t}\left(\frac{\partial \zeta}{\partial \omega}\right) = \frac{\partial}{\partial x}\left(\frac{\partial \zeta}{\partial k}\right),$$

and another one yields a dispersion relation $\omega = \omega(k, \eta)$. The appearance of amplitude dependency in the dispersion relation is the main non-linear effect of dispersive systems. When a reference frame can be found in which the modulation parameters are stationary (we use one travelling upward with the nose of the plug), we immediately have:

$$\omega = \omega(k, \eta) = \text{constant}$$
$$\frac{\partial \zeta}{\partial k} = \text{constant}.$$

Adopting the near-linear Stokes expansions for φ, Whitham (1974, p. 554) applied the above equations to the case of gravity waves along a non-uniform current in shallow water. The case when surface tension is the only compensating force is now treated along similar lines. Note that the influence of gravity is small as compared to the acceleration of the flow in the short nose of the plug. Neglecting gravity and induced mass flow effects one obtains :

$$\zeta = 0.5\ W\ [\ (\omega - kU_o)^2/\omega_o^2 - 1] + O(W^2)$$
$$\omega \approx kU_o(z) + \omega_o$$
$$\frac{\partial \zeta}{\partial k} = W.\left(U_o + \frac{d\omega_o}{dk}\right)/\omega_o + O(W^2)$$

where the uniform velocity of the current is denoted by U , $W = \frac{1}{2}k^2\eta^2\sigma$ and $\omega_o = \{\frac{\sigma}{\rho} k^3\ \mathrm{tgh}(kh)\}^{1/2}$. In solving these equations second and higher orders of W are neglected. Let $\underline{c}$ be the solution of the implicit equation:

$$\underline{c}^3 = (1 - U_o/\underline{c})^{-2}\ \frac{\sigma}{\rho}\ \omega\ \mathrm{tgh}\ (\omega h/\underline{c})$$

and let V denote $3(c - U)/2 + \omega h/\sinh(2\omega h/(c-U))$. The square of the amplification factor η_2/η_1 for the amplitude as a wave travels from location 1 to 2 can then be expressed in the form :

$$(\eta_2/\eta_1)^2 = (\underline{c}_2/\underline{c}_1)^2 \frac{(V_1+U_{o_1})}{(V_2+U_{o_2})} \frac{(1-U_{o_2}/\underline{c}_2)}{(1-U_{o_1}/\underline{c}_1)}$$

These equations were solved numerically to study the development of a disturbance originating from the nose of the plug. Typical outcomes are :

h_1	h_2	U_1	$2\pi/\omega$	k_2	η_2/η_1
5	1	1	7	178	2.5
10	1	1	8	78	11.5
mm	mm	m/s	ms	m^{-1}	-

We can conclude that an initially small disturbance can be effectively enlarged by the acceleration of the main stream near the nose of the plug. In most cases the amplification factor η_2/η_1 is much larger than the value $\sqrt{2}$, approximately valid for gravity waves on a beach without a current (Lighthill, 1978 ,p. 258).

For waves of moderate amplitude, there is a type of instability that is not related to the core flow and hence has no direct bearings on the P-C transition. In the following, this instability is qualitatively considered, and again an indication about the kind of waves involved in the transition is obtained.

Gravitational nonviscous waves of moderate amplitude are found to be weakly unstable in the sense that small, gradual modulations to the wave grow, (Benjamin, 1967, Whitham, 1974). These modulations may develop spontaneously from background hydrodynamic noise and gain energy from the primary wave motion. By a proces of selective amplification a pair of side-band modes emerges with a frequency shift with respect to the fundamental frequency already present. The elliptic form of the governing equations for these

modulations does not refer to a chaotic motion, but rather implies that the modulation becomes more pronounced the farther the wave travels. The phenomenon is also demonstrated experimentally, (Feir, 1967), and is predicted when $k\eta < 0.57$ and $kh > 1.363$. The situation for a vertical strong current (velocity has order of magnitude 3 m/s) has different aspects, as we shall see presently, but it is safe to conclude, that there may exist a lower bound on the value of $k\eta$ that can be used in the analysis of finite amplitude waves in the following chapter.

The growth of waves can originate from evolving modulations or from acceleration of the main stream, but also from interaction with the core flow. The latter cause is the one that will be investigated in this paper. As indicated before, large amplitude waves are involved in the P-C transition, whence a linear theory is inappropriate. The motion of the vapor pocket as a whole manifests itself to the liquid film via the core. Insofar the liquid film is moving down freely, i.e. due to gravity forces counteracting (turbulent) viscosity, wall friction and interfacial stresses, stability is governed by the interaction with the core flow.

1.1.3 Modelling considerations. We do not wish to pursue a variational approach to the growth of disturbances such as has been done in 1.1.2. Not only can it not be pointed out exactly where waves are initiated in the nose of a plug, which makes it less useful to study wave development, but also instability phenomena, that are already apparent in absence of a gas/vapor flow, unavoidably show up again in a more general analysis for growing waves that also includes interaction with the environment. By avoiding such generality, the already intricate calculations are not made overcomplicated. Furthermore it is undesirable to study an explicit dependency on the plug length, since calculations of this length are not very accurate, as we shall see in section 3.1. Such a dependency is due to the time (or distance) it takes for a wave or instability to develop, and hence is introduced whenever wave development is studied. Moreover, an appropriate variational approach not only requires additional terms representing a dependence on rate of change of amplitude (Davey, 1974). It would also require a Lagrangian that contains boundary conditions influenced by the non-conservative interaction

with the gas core. In addition, an exact expression or at least a meaningful expansion for the periodic part of the velocity expression in such a Lagrangian would be required. Such a Lagrangian is not known to the author for the strictly non-linear, moderately dispersive shallow water case at hand, even if the interaction with the core were left out.

The degree of "shearing" or amplitude dispersion can easily be estimated from the parameter $\eta.\lambda^2/h^3$. Solutions of the non-linear Korteweg-de Vries equations show, that when this parameter exceeds a value of about 16 waveform shearing by non-linear effects proceeds to steepen the front of the wave (Lighthill, 1978). Typical values of this parameter for the case of a rising plug are in the range [16,100], so waveform shearing might become significant then. This amplitude dispersion amounts to a positive rate of introduction of a sin(2kz) component (see figure 2 for example), whence such a component is taken along in the current treatment. Though we shall start with some sort of expansion for the velocity potential, it shall only be used to approximate the real velocities locally. To be precise, in the neighbourhood of only a few locations. In other words, an attempt is made to derive a dispersion relation without knowing an exact describing wave equation. The shearing is represented by a factor F , which can be estimated.

Dispersive equations, defined as corresponding to a dispersion relation with a non-constant group velocity $\frac{d\omega}{dk}$ for almost all wavenumbers, are in general elliptic. In a loose sense this can be demonstrated by noting that each value for a variable u_i can correspond to infinitely many (phase) velocities c. Non-dispersive non-linear equations have only one velocity c_i corresponding to each value of u_i. One can obtain a hyperbolic set of equations for dispersive systems by selecting other basic parameters, one of them being the wave number (Whitham, 1974).

Problems arise when it is necessary for averaging procedures to relate an average of products of dependent variables to the product of averages. Such is the case, for instance, when the velocity profile is non-uniform, and then the introduction of various distribution coefficients is required; see Banerjee and Chan (1980). However, these coefficients merely shift the problem to the transfer relations between the phases. In the example of plug flow, the two phases are liquid film and gas core. Their mutual interaction depends on the amplitude of the disturbances, or, to put it differently, on

the penetration depth, which makes it hard to find appropriate transfer relations ab initio. We may note that in some other practical examples (Analytis and Lübbesmeyer, 1983), it is useful to split up a nonuniform distribution into two or more distinct main parts. Each part gets its own independent variable corresponding to the averaged value of some former parameter that was approximately constant in that part. In these cases the problem of non-uniform profiles can be dealt with, and complex characteristics may indicate instability (Saito, 1977).
The main difference of the present analysis with the Helmholtz treatment, apart from the appearance of finite amplitude waves, is the fact that the (undisturbed) velocity profile for the core is taken to be non-uniform. The internal circulation is represented in an approximate way by a parabolic velocity profile. This essentially non-uniform profile, but also the effective dispersion (one expects $\lambda < 5$ cm and a liquid film thickness of the order of 1 mm), imply that it is practically impossible to predict the P-C-transition by evaluating the characteristics of a common set of conservation equations that are supposed to be valid for many kinds of two-phase flows and are averaged in some way or another. An example of such a set is given by the two-fluid model of Ishii (1975). One of the shortcomings of two-fluid models is that they are designed to be equally well applicable to all possible flow patterns.

Two general remarks conclude these modelling considerations.
Whitham (1974) and Longuet-Higgins (1975) showed that imaginary characteristics do not have to refer to chaotic motions, but rather to large deviations from the uniform state. Since P-C flow pattern transition cannot be sharply defined as will be demonstrated in 3.3, this observation is of less importance for the present investigation.
Bryce (1977) for example attempted to improve on universal void correlations by creating real characteristics for averaged two phase flow equations. The considerations of this section show that one should question the physical significance of such a procedure when elementary phenomena as dispersion, diffusion and inhomogeneous distributions are not accounted for properly. Imaginary characteristics may indicate flow regime transition. When a void correlation obtained by forcing real-valued characteristics is supposed to

be applicable to different flow regimes relevant physical information is probably suppressed artificially.

1.2 Outlines of the treatment

To allow for some diffraction of wave energy the physical propagation space is taken to be a Riemann space. As explained in 1.1.3 wave development is not studied explicitly. Because of the momentary character of wave observation and the assumption that parameters as the mean liquid film thickness vary only gradually, wave propagation is studied in the tangent space (z,y,t,k). The phase α and wave number k are defined in the same way as described in 1.1.2. Assuming rotational symmetry we use the space (z,r,t,k) for the core flow. The tube radius is taken to be that large, that for the liquid film a rectangular coordinate system (x,y,z) is appropriate. Subsequently the x-dependency is suppressed, whence treatment becomes essentially two-dimensional. See figure 1 for the definition of coordinate systems. If wave diffraction or a progressive evolution is effective, the waveforms exhibited in figures 2, 5 and 6 are to be seen as periodic extensions of an isolated disturbance, and not as a wavetrain actually present. According to well-known solutions of the non-linear Korteweg-de Vries equation differences between humps of wavetrains and isolated humps vanish at the modelling level, whenever large amplitudes are involved (Lighthill, 1978).

For reasons explained in 1.1, attention is focussed on large amplitude waves. The pseudo-amplitude A is varied to study the effects of interaction with the core flow. Here A is a pseudo-amplitude because of the fact that it appears only implicitly in the equations, and because of the contribution of the imaginary part of the wave frequency to the real amplitude via a factor $\exp(\mathrm{Im}(\omega)\, t)$. In another part of the analysis, several fixed values for $k\eta$ are fed into the equations to show that the resulting stability calculations and flow regime predictions are hardly dependent on the value for $k\eta$ within the theoretical limits that shall be derived. These limits shall be compared with the expectations following from the conclusions in 1.1.2.

As explained in 1.1.3, the effective "shearing" of wave amplitude may not be balanced completely by dispersion and energy diffusion. The instantaneous rate of shearing is introduced in the analysis via a $\sin(2kz)$ component in a

sort of expansion that is used to approximate the velocity potential locally. The results are found to be only slightly sensitive to the estimated value of the factor F, that quantifies the amount of amplitude dispersion. An exact determination of F would have been possible by selecting values for the superficial velocities and by iterating the, already time-consuming, stability calculations in order to determine the local phase velocity c. This was unnecessary at the present level of approximations and has been omitted in favour of practical equations for flow regime prediction.

A reference frame is chosen in which, in the absence of amplitude dispersion (i.e. when F = 0), a crest of a wave would appear at z = 0. Such a frame has to move with the phase velocity c with respect to the main stream. The latter has a velocity U in the laboratory frame in which the tube is at rest (see figure 1). U is assumed to be large as compared to the velocity of the stream induced by the wave motion. Hence the induced stream can be neglected in first approximation. The growth of waves is assumed to be controlled initially by linearized theory. Energy will then collect into a neighbourhood of that wavenumber k_o that makes the imaginary part of ω a maximum (see Whitham, 1974, for example). Hence k_o follows from :

$$\frac{d}{dk} \Big|_{k_o} k \, \mathrm{Im}(c) = 0$$

In the next sections the algebra is suppressed as much as possible in order to highlight the calculation procedure and the results, including dependencies on physical parameters. As explained in 1.1.1, churn flow is predicted when the liquid film of a supposed plug is found to be unstable.

In 3.1 a calculation procedure for the flow pattern is presented, and, using this procedure, in 3.2 the results of chapter 2 are compared with experimental results. In 3.3 the question will be answered whether churn flow stabilizes into plug flow or plug flow evolves into churn flow.

2 STABILITY CALCULATIONS

2.1 Film flow

2.1.1 Undisturbed flow. The undisturbed liquid film is considered to be adjacent to the wall with a single free interface (see figure 1 for definition of coordinate systems). We consider the flow in the part remote from the wall only, where boundary layers are not of importance. The net force decelerating the fluid follows from

$$(1) \quad \nu \, \underline{u} \, (\nabla^2 \, \underline{u}) = \underline{u}.\underline{\nabla} \, \{\tfrac{1}{2} \, q^2 + \frac{p}{\varrho} + gz\}$$

Here ν includes turbulent viscosity. We split up the velocity $\underline{u}$ in an undisturbed part $\bar{\underline{u}}$ (or $\bar{u}$) and the disturbancy part $\hat{\underline{u}}$ (or $\hat{u}$). Neglecting the vorticity generated near the free surface we take

$$(2) \quad \underline{\nabla} \times \hat{\underline{u}} = 0$$

Hence we can introduce a velocity potential φ to describe disturbances. With the equation of continuity now follows

$$(3) \quad \nabla^2 \, \hat{\underline{u}} = -\underline{\nabla} \times (\underline{\nabla} \times \hat{\underline{u}}) = 0$$

Neglecting gradients in the z-direction of both pressure and velocity squared in (1) we obtain:

$$(4) \quad \underline{u}.\underline{\nabla}gz = -\underline{u}.\underline{g} = \nu \, \underline{u}.(\nabla^2 \bar{\underline{u}})$$

where use has been made of (3). Applying Green's first identity to the resulting equation

$$-g = \nu \, \nabla^2 \, \bar{u}$$

we find for each angle $d\kappa$, for all $R_1 < R$ and for all $r < R_1$

$$(5)\quad -\int_{\text{volume}} dz\, 2\pi r\, dr\, d\kappa\, g = \int_{\text{surface}} d\underline{a}\, \nu\, \underline{n}.\underline{\nabla}\, \underline{\bar{u}} =$$

$$= (\nu \frac{\partial}{\partial r}\Big|_r \bar{u}\, r - \nu \frac{\partial}{\partial r}\Big|_{R_1} \bar{u}\, r)\, d\kappa\, dz$$

where the invariance under translations in the z-direction has been further exploited.
When interfacial stresses do not occur we conclude

$$(6)\quad \frac{\partial \bar{u}}{\partial r}\Big|_r = (-\frac{\varrho g}{2\mu})\,[r^2 - (R-h)^2]\,\frac{1}{r}$$

In the appendix, equation (6) is used to derive a relation between the mean fluid velocity U and the mean film thickness. This relation will be used in section 3.1 to predict flow regimes. The correction factor K_2 derived in the appendix is a good measure for the correctness of the assumption $h \ll R$ (if correct then $K_2 \approx 1$).

2.1.2 Disturbances. The disturbances are considered to take the form of waves of finite amplitude (see 1.1.). In analogy with the case of a simple harmonic progressive wave hyperbolic functions are used to assure a zero velocity at the wall. We try to fit the parameters that are constant in a potential of the form

$$(7)\quad \varphi = \sum_i c_i \cosh(k_i\,(y+h))\,\sin(\sigma_i\, t + n_i\, z + \varphi_i)$$

It is taken, that $h \ll R$ and that (z, y) is a rectangular coordinate system (see section 1.2.).
From Laplace's equation $\Delta\varphi = 0$ follows $n_i = k_i$. For a second order approximation we truncate after two terms. A reference frame is chosen that travels with the crest of the wave. As explained in chapter 1 we do not want to study wave development explicitly. However, one is able to account for the instantaneous rate of amplitude shearing by taking $\sigma_1 \approx \sigma_2$ and $\varphi_2 - \varphi_1 = \pi$. This will be elucidated in 2.2.. Let c denote the phase velocity relative to the laboratory-frame in which the tube is at rest. Let $U = v = \pm|\bar{u}|$ (+ if upward flow). The wave number k shall be determined by differentiation with

respect to k of an expression containing e.g wave-amplitude. The constants c_i are modified in order to make the wave-form and wave-amplitude hardly dependent on the k :

$$(8)\quad \psi = (U+c)y - (U+c)A\cos(kz)\left[\left\{\frac{\sinh(ky+kh)}{\sinh(kh)}\right\} + - \left\{\frac{\sinh(2ky+2kh)}{\sinh(2kh)}\right\} 2F\sin(kz)\right]$$

In this stream function, ψ the disturbances have been recombined with the undisturbed flow that is represented by the first term on the RHS. At the interface, where we write $y = \eta$, we can take $\psi = 0$. This yields:

$$(9)\quad \eta = A\cos(kz)\{((6))^{-1} - ((1))\,2F\sin(kz)\}$$

which is implicit in η. Examples of waves obtained with (9) are given in figure 2. Throughout this paper the following short-hand notation is used:

$$\begin{aligned}
(10)\quad ((1)) &= \sinh(2kh + 2k\eta)/\sinh(2kh)\\
((2)) &= \cosh(kh + k\eta)/\sinh(kh)\\
((3)) &= I_1(2\,k\theta)/I_1(2kh')\\
((4)) &= I_0(k\theta)/I_1(kh')\\
((5)) &= \cosh(kh + k\eta)/\cos(kh)\\
((6)) &= \sinh(kh)/\sinh(kh + k\eta)\\
((7)) &= \sinh(kh + k\eta)/\cosh(kh)\\
((8)) &= I_1(k\theta)/I_1(kh')\\
((9)) &= I_0(2k\theta)/I_1(2kh').
\end{aligned}$$

in which I_0 and I_1 are modified Bessel functions of order 0 and 1 respectively, and in which

$$(11)\quad \theta = h' - \eta = R - h - \eta$$

Taking advantage of symmetry and applying the first theorem of integral calculus to the equation of continuity in integral form, one derives the kinematic surface condition for finite amplitude waves:

$$(12)\quad v_r(\theta) + v_z(\theta)\,\frac{\partial \eta}{\partial z} + \frac{\partial \eta}{\partial t} = 0$$

With a stationary interface this reduces to

$$(13)\quad \eta' \overset{\text{def}}{\equiv\equiv} \frac{\partial \eta}{\partial z} = \left(-\frac{\partial \psi}{\partial z}\right)/\frac{\partial \psi}{\partial y}$$

from which follows:

$$(14)\quad \eta'\left(1 - k\eta\,\frac{[\,((2)) - 4F\sin(kz)\cosh(2kh + 2k\eta)/\sinh(2kh)\,]}{[\,((6))^{-1} - ((1))\,2F\sin(kz)\,]}\right) =$$

$$= -k\eta\,\mathrm{tg}(kz) - 2\,A\,k\,F\cos^2(kz)\,((1))$$

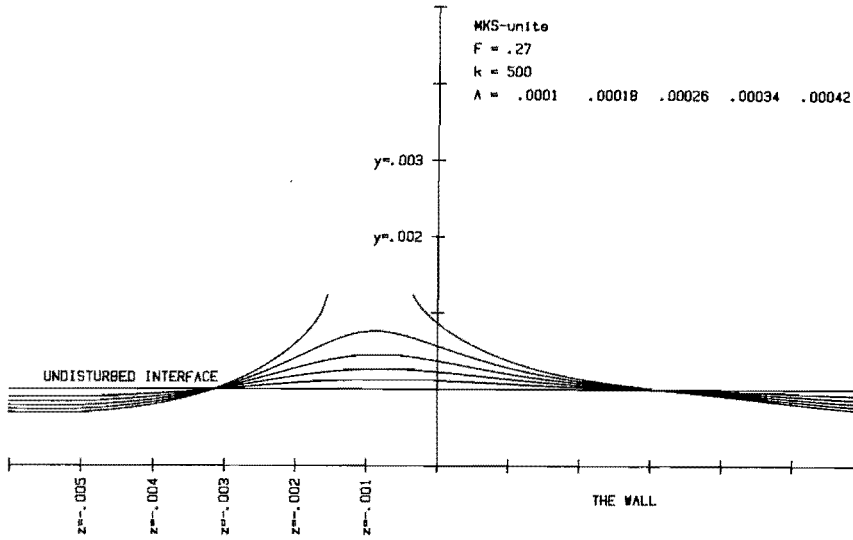

Figure 2

Examples of waves with different amplitudes (k=500 ; F=0.27)

Later we shall need (14), which can also be derived from (9) by implicit differentiation. In the latter way $\eta'' \equiv \frac{\partial^2 \eta}{\partial z^2}$ follows from equation (14). This provides us with the following set of equations:

$$(15)\quad \eta''\,(\sin(kz) = \pm 1) = 2\,A^2\,k^3(\pm 1\text{-}2F)(\pm \mathrm{ctgh}(kh) - 4F\,\mathrm{ctgh}(2kh))$$

and, for η'' evaluated at points where cos(kz) is equal to 1 :

$$(16)\quad \eta''(\cos(kz) = 1) = A\,k^2\,(k\eta\ \mathrm{ctgh}(k\eta + kh)-1)^{-2}\{k\eta\ \cosh(k\eta + kh)+ -\sinh(k\eta + kh)+ 8\,F^2\,k\eta\ ((5))\ \cosh(2kh + 2k\eta)/\sinh(2kh) + + 4F^2 k\eta\ ((1))\ ((5))\ (k\eta\ \mathrm{ctgh}^2(kh + k\eta) - \mathrm{ctgh}(kh + k\eta) + -k\eta)/(k\eta\ \mathrm{ctgh}(kh+k\eta) - 1) + 4\,F^2\,k\eta\ ((1))\ ((7))\ \}$$

Furthermore, from (14) :

$$(17)\quad \eta'\ (\cos(kz) = 1) = 2\,F\,k\eta\ ((5))\ /(k\eta\ \mathrm{ctgh}(kh + k\eta) - 1)$$

$$(18)\quad \eta'\ (\sin(kz) = \pm\ 1) = -A\,k\ (\ \pm\ 1 - 2F)$$

with

$$(19)\quad \eta\ \ (\cos(kz) = 1) =\ A\ ((6))^{-1}$$

The following conclusion can already be drawn from (16) and (17): it is not permitted to neglect surface tension forces, proportional to η'' , if one takes the limit

$$(20)\quad k\eta\ \mathrm{ctgh}(k\eta + kh) \to 1$$

for waves showing $z = 0$ as a point of symmetry. For in that case $F = 0$, $\eta'(z=0) = 0$ and :

$$(21)\quad \eta'' = Ak^2\ \sinh(kh + k\eta)/(k\eta\ \mathrm{ctgh}(k\eta + kh) - 1),$$

which takes values that cannot be neglected. This case will be considered in 2.4.3.

2.2 Core flow

2.2.1 Introduction. In stability calculations of the Helmholtz type, two concurrent liquid layers are considered, which by external causes are forced to move at different speeds. Here we study a liquid film and a gas/vapor core with motions that are connected with each other. Within a plug or Taylor bubble, internal circulation is present, since the drag exerted by the falling liquid film causes a downward motion of the gas/vapor close to

the film. Hot wire anemometer experiments and smoke tests (Filla, Davidson, Bates & Eccles, 1976) reveal circulating vortices. In long plugs, i.e. $L_p > 4D$, several toroidal vortices may occupy the gas/vapor core. Because of the falling liquid film circulation is always present, and the mean velocity profile has to account for this. In the following, a derivation is presented for a realistic velocity profile for the undisturbed core flow. Since the motion of the air/vapor near the liquid film is largely determined by this film itself, it cannot be expected that instability of waves at the interface occurs as easy as in the usual Helmholtz theory (see also 1.1.1). It will be shown here that instability only occurs when the amplitude of the wave is that large, that it can be affected by internal motions of the toroidal vortex, which have higher velocities relative to the liquid surface.

2.2.2 Derivation of the stream function. Let the undisturbed flow of the core be described by the stream function $\bar{\psi}'(r)$, and the total flow by

$$(22) \quad \psi' = \bar{\psi}'(r) + \hat{\psi}_1'(r)\cos(kz) + \hat{\psi}_2'(r)\, F \sin(2kz)$$

from which the velocities v_z' and v_r' can be deduced with the aid of

$$(23) \quad v_z' = \frac{1}{r}\frac{\partial \psi'}{\partial r} \quad ; \quad v_r' = -\frac{1}{r}\frac{\partial \psi'}{\partial z}.$$

The Navier-Stokes equations and the description of the interface given by (9) will be used to derive relations which determine $\bar{\psi}'$ and the $\hat{\psi}_i'$.
The equations for incompressible core flow, written in dimensionless form, read:

$$(24) \quad \underline{u}' \cdot \underline{\nabla}\, \underline{u}' + \frac{\partial}{\partial t}\underline{u}' = -\underline{\nabla}\, p' + \frac{\bar{g}}{U'^2} L + \frac{1}{R_e}\Delta\, \underline{u}'$$

in which R_e denotes the Reynolds number, L a characteristic distance and U' a characteristic velocity; $\underline{u}' = \underline{v}'/U'$ for instance. Dynamic viscosity μ may include a turbulence part. A turbulent motion is considered with R_e high

enough to allow abortion of the last term on the RHS of (24). For rotatory-symmetric flows in our frame of reference, the following set of equations results:

$$(25)\quad v_r' \frac{\partial}{\partial r} v_z' + v_z' \frac{\partial}{\partial z} v_z' = - \varrho'^{-1} \frac{\partial p'}{\partial z} + g$$

$$(26)\quad v_r' \frac{\partial}{\partial r} v_r' + v_z' \frac{\partial}{\partial z} v_r' = - \varrho'^{-1} \frac{\partial p'}{\partial r}$$

Substituting (22) and (23), we differentiate (25) with respect to r, and (26) with respect to z. Substraction of the resulting two expressions for $\varrho^{-1} \frac{\partial}{\partial r} \frac{\partial}{\partial z} p'$ from each other yields:

$$(27)\quad - \frac{k}{r} (\psi_1' \sin(kz) - 2 F \cos(kz) \psi_2') \{ \frac{1}{r} \frac{\partial \bar{v}_z'}{\partial r} - \frac{\partial^2 \bar{v}_z'}{\partial r^2} \} +$$

$$+ \bar{v}_z' \frac{k}{r} \sin(kz) \{ \frac{1}{r} \frac{\partial \psi_1'}{\partial r} - \frac{\partial^2 \psi_1'}{\partial r^2} + k^2 \psi_1' \} +$$

$$+ v_z' \cos(2kz) \frac{2k}{r} F \{ - \frac{1}{r} \frac{\partial \psi_2'}{\partial r} + \frac{\partial^2 \psi_2'}{\partial r^2} - (2k)^2 \psi_2' \} + \Gamma = 0$$

in which Γ is a lengthy expression containing "mixed" terms with factors like sin(kz).cos(kz). Since (27) must hold for arbitrary kz, F and $\bar{v}_z'(r=0)$ we deduce:

$$(28)\quad \frac{1}{r} \frac{\partial \bar{v}_z'}{\partial r} - \frac{\partial^2 \bar{v}_z'}{\partial r^2} = 0$$

$$(29)\quad \frac{1}{r} \frac{\partial \psi_j'}{\partial r} - \frac{\partial^2 \psi_j'}{\partial r^2} + (jk)^2 \psi_j' = 0$$

(j=1 or 2). Differentiating (29) with respect to r, an expression is obtained for $\frac{\partial^3}{\partial r^3}\ \hat{\psi}'_j$, which can be used to show that Γ equals zero when (28) and (29) hold.
The vorticity ω is given by

$$(30)\quad \omega = \frac{1}{r}\left(\frac{\partial^2}{\partial r^2}\psi' - \frac{1}{r}\frac{\partial}{\partial r}\psi' + \frac{\partial^2}{\partial z^2}\psi'\right)$$

which on account of (29) equals zero for the disturbancy part. In the derivation of (28) and (29), no assumption has been made regarding the magnitude of perturbed quantities. So the equation derived is valid for all amplitudes of waves considered.
The general solution of (29) is

$$\hat{\psi}'_j = A'\ r\ I_1(jkr) + B'\ r\ K_1(jkr).$$

Axial symmetry demands $v'_r\ (r=0) = 0$, whence $B' = 0$ and

$$(31)\quad \hat{\psi}'_j = A'\ r\ I_1(jkr)$$

The general solution of the homogeneous differential equation (28) is given by

$$(32)\quad \bar{v}'_z = q_o + q_2\ r^2$$

Defining v as the velocity of the surface and v'_c as the velocity at the center of the tube, this yields in our frame of reference, h' being equal to R-h:

$$(33)\quad v'_z = v'_c + c + h'^{-2}\ r^2\ (v-v'_c)$$

Equations (32) and (33) are considered as a first approximation to the real velocity profile in the core (see 1.1.3). As noted before, they express internal circulations in a Taylor bubble. Obviously the case at hand is physically quite different from the case of a uniform turbulent stream of air flowing along a liquid interface. Hence the use of the universal

velocity distribution is inappropriate. Clearly the no-slip condition between the gas/vapor and the liquid demands the presence of some laminar sublayer. Also, some part of the gas rises at a velocity larger than the velocity of the front of the liquid slug. The gas within the Taylor bubble has a velocity distribution to which equation (33) represents a first estimate.

In general a stream function is determined up to a gauge constant. Here we have to determine this constant in accordance with (9). So if we want to describe the interface by $\psi' = 0$, (33) yields

$$(34)\quad \bar{\psi}' = (c + v_c')\,\frac{1}{2}\,(r^2 - h'^2) + (v - v_c')h'^{-2}\,\frac{1}{4}\,(r^4 - h'^4)$$

since $\psi' = \bar{\psi}'$ in the case of neglectably small disturbances. Again making form and amplitude of the wave almost independent of the wave number, we transform (22) into:

$$(35)\quad \psi' = -\frac{1}{2}\,h'^2\,(c+v_c') - \frac{1}{4}\,h'^2\,(v-v_c') + (c+v_c')\,\frac{1}{2}\,r^2 +$$

$$+ h'^{-2}(v-v_c')\,\frac{1}{4}\,r^4 + A''\,\frac{r\,I_1(kr)}{I_1(kh')}\cos(kz) +$$

$$- A''\,F''\,\frac{r\,I_1(2kr)}{I_1(2kh')}\sin(2kz)$$

and the interface is described by

$$(36)\quad 0 = \frac{1}{2}\,(v_c' + c)\,(-2h'\eta + \eta^2) + \frac{1}{4}\,h'^{-2}(v-v_c')\,(\eta^4 - 4h'\eta^3 - 4h'^3\eta +$$

$$+ 6h'^2\,\eta^2) + A''(h' - \eta)\,((8))\cos(kz) +$$

$$- A''\,F''\,(h' - \eta)\,((3))\sin(2kz).$$

2.2.3 Determination of A" and F". At points where cos (kz) = 0 (36) and (9) coincide by our choice of the gauge constant. By letting (36) and (9) coincide for some other specific values of kz, relations are obtained between the pairs (A", F") and (A, F). Since $\eta(\cos(kz) = 0) = 0$ and the

waveform is supposedly continuous, the inequality $|\eta| << 1$ holds when $|\cos(kz)| << 1$. Using the latter inequality from (9) then follows

$$\eta \approx A \cos(kz) \, (1-2 F \sin(kz))$$

which substituted in (36) with neglection of the highest powers of η yields

$$0 \approx -h' \{ A(c+v) \, (1-2F \sin(kz)) - A" \, (1-2F" \sin(kz)) \} + \\ - A" \cos(kz) \, (1-2F" \sin(kz)) \, A \, (1-2 F \sin(kz)).$$

This gives

$$(37) \quad \frac{(c+v)A}{A"} \approx \frac{1-2F"}{1-2F} \stackrel{def}{\equiv\equiv} \frac{1}{f}$$

or, writing (37) differently

$$(38) \quad F" = \frac{1}{f} F + \frac{1}{2}(1 - \frac{1}{f}) \quad ,\text{and}$$

$$(39) \quad A" = f(c+v)A.$$

Now the set (A", F") is determined by (A, F, f). When (38) and (39) hold, $\eta'(\cos(kz) = 0)$, as derived from (36), is identical to the $\eta'(\cos(kz) = 0)$ as given by (9); a similar conclusion holds for $\eta"(\cos(kz)) = 0)$. This value of η' and the one of $\eta"$ will be used in the derivation of an expression for F in terms of (V+c) and A.

Since an important dispersion relation results from a force balance at a point near the crest of the wave, we now consider this point, given by $\cos(kz) = 1$, in order to determine f. Implementing $\eta = A/ ((6))$, as obtained from (9), in (36) we get

$$A"/A = [\frac{1}{2} (v_c'+c) \, (-2h'+\eta) + \frac{1}{4}h'^{-2}(v-v_c') \, (\eta^3-4h'\eta^2-4h'^3 + \\ + 6h'^2\eta)]/\{ ((6)) \, ((8)) \, (\eta-h') \},$$

which after combination with (39) gives

$$(40)\quad f = \left[1 - \frac{(v-v')}{(v+c)}\frac{c}{}\,\frac{\eta}{h'}\,\frac{(h'-\frac{1}{2}\eta)^2}{h'(h'-\eta)}\right] / \{\,((6))\,((8))\,\}.$$

In accordance with our assumption h << R, or h<<h', we neglect in (40) the term proportional to $(v-v_c')$, whereby must hold:

$$(41)\quad (v + c) \neq 0$$

$$(42)\quad f \approx \{\,((6))\,((8))\,\}^{-1},$$

with the $k\eta$ that occurs in ((6)) and ((8)) (see (10)) being given by the equality $kA.\sin(kh + k\eta)/\sinh(kh) = k\eta$.

2.2.4 Determination of F. We shall now use Bernoulli's equation at points where sin(kz) = -1 to derive the equation for F already mentioned in 2.2.3. At each point of the interface, the pressures p and p' are connected via

$$(43)\quad p - p' = -\sigma\,\eta^*\,(1+\eta'^2)^{-3/2} - \sigma/\theta.$$

Since Bernoulli's equation determines the pressure up to a constant, we shall use (43) at points where sin(kz) = +1 to fix the resulting constant in p-p'.
From Euler's law of motion, one derives the well-known equation

$$(44)\quad \frac{\partial}{\partial t}\,\underline{q}' - \underline{q}'\times(\underline{\nabla}\times\underline{q}') = -\underline{\nabla}\{\,\frac{1}{2}\,q'^2 + gz + \int \varrho'^{-1}\,dp'\}$$

where $\underline{q}'$ denotes the velocity vector. In the present case the core flow is only rotational due to the undisturbed part, and with aid of (34) it can be shown that $\underline{q}'\times(\underline{\nabla}\times\underline{q}')$ is proportional to (see also figure 1)

$$\hat{r}\,\frac{\partial}{\partial r}\,\psi' + \hat{z}\,\frac{\partial}{\partial z}\,\psi' = \underline{\nabla}\,\psi'$$

Since, at a streamline, ψ' is a constant with the aid of (44) we arrive at Bernoulli's equation for incompressible media in the stationary case:

$$(45)\quad \varrho^{-1}p' = -\frac{1}{2}v'^2 - gz + \text{Constant}.$$

A similar equation holds for the pressure in the liquid film.
Define λ_+ and λ_- by

$$(46)\quad \lambda_{\pm} = \eta''\,(\sin(kz) = \pm 1)\ .\ \{1 + \eta'^2(\sin(kz) = \pm 1)\}^{-3/2}$$

where η' and η'' are given by (19) and (15).
The constant in (45) is now fixed in such a way, that at points where $\eta = 0$ and $\sin(kz) = 1$ the dynamic pressure $p - p'$ equals zero when there are no disturbances:

$$(47)\quad p\,(\sin(kz)=1)\varrho^{-1} = -(v+c)^2\,\frac{1}{2}\,[k^2A^2(1-2F)^2+1] + gz$$

$$p'(\sin(kz)=1)\varrho'^{-1} = -(v+c)^2\,\frac{1}{2}\,[1+f^2A^2k^2(1-2F'')^2] + @\varrho'^{-1}+gz$$

with @ such that (43) holds at kz where $\sin(kz)=1$. This fixes @ only in terms of F. Parameter F is now determined by relating $p-p'$ of points where $\sin(kz)= -1$ to $p-p'$ of points at half a wavelength distance (where $\sin(kz)= +1$). This yields :

$$(48)\quad -\varrho g\,\frac{\pi}{k} + \varrho' g\,\frac{\pi}{k} + (v+c)^2\,\frac{1}{2}\,k^2A^2(8F\,\varrho - 8F''\,\varrho'\,f^2) - \sigma(\lambda_- - \lambda_+) = 0$$

Notice that in the undisturbed case gravity acceleration is counterbalanced by (viscous or turbulent) dissipation and boundary stresses, as already indicated in (4). To some extent this also holds when disturbances are present, whence we use (48) only to estimate F and otherwise neglect the gravity term in the Bernoulli equation. After estimating F in this way, it is then supposed that (43) is approximately valid for all of z. From (48) is derived :

$$(49)\quad F = \frac{\sigma}{2(\varrho-\varrho'f)}\ \frac{k\,\Gamma_o}{(v+c)^2} + \frac{(\varrho-\varrho')}{(\varrho-\varrho'f)}\left(\frac{1}{4k^2A^2}\,\frac{1}{k}\,\frac{\pi g}{(v+c)^2}\right) +$$

$$+ \frac{1}{2}\,f(f-1)\,\frac{\varrho'}{(\varrho-\varrho'f)}$$

with

$$(50)\quad \Gamma_o = (1+2F)\,(\mathrm{ctgh}(kh) + 4F\,\mathrm{ctgh}\,(2kh))\,(1+A^2k^2(1+2F)^2)^{-3/2} +$$

$$- (1-2F)\,(\mathrm{ctgh}(kh) - 4F\,\mathrm{ctgh}\,(2kh))\,(1+A^2k^2(1-2F)^2)^{-3/2}$$

Since $\Gamma_o = \Gamma_o(F)$, (49) is impliciet in F. When $k\to\infty$, it follows from (41) and (49) that $F \to 0$ (for if not, then $\Gamma_o \neq 0$). This is what one expects. Only waves with relatively long wavelengths are affected by gravity. Relative to the troughs their crests have a tendency to bend in the direction of the gravity vector, since when $\lambda_+ > \lambda_-$ also $F > 0$. This effect is enhanced by the relative motion of the waves, as indicated by the factor $(\varrho-\varrho' f)\,(v+c)^2$ on the R.H.S. of (49). However, if we were to blow a rapid stream of air along a cylinder of water according to the estimation of F given by (49) the same tendency and similar slopes of the water interface are observed, since $\varrho \ll \varrho'$ and $F < 0$ in that case. Since this is exactly what one expects on intuitive grounds, equation (49) is considered to furnish valuable information concerning the amount of amplitude dispersion as represented by the parameter F (see also 1.1.3).

When $\eta = 0$, it follows from (9) that either $\cos(kz) = 0$ or $|F| > \frac{1}{2}$. Since in the latter case "false" wavecrests (i.e. not separated by a distance λ) appear, we take by convention :

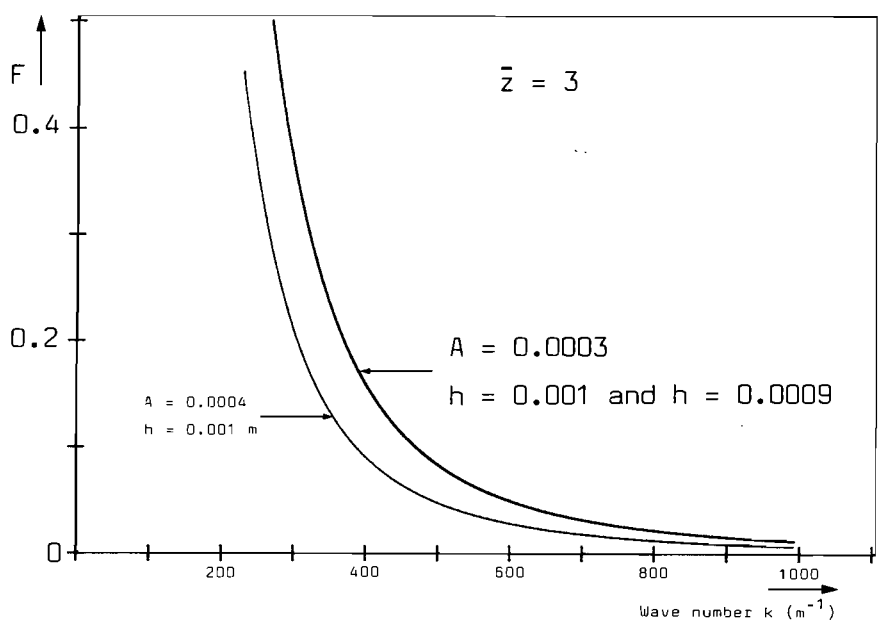

Figure 3
Dispersion factor versus wave number

(51) $|F| < \frac{1}{2}$

For the air-water properties $\varrho = 1000$, $\varrho' = 1.18$ and $\sigma = 0.073$ (MKS units), which will be referred to as the "standard" set of physical parameters, in figure 3, F is shown as a function of k. Apart from the above mentioned $\lim_{k\to\infty} F = 0$ two other trends are obvious from (49):

(52) $A_1 > A \rightarrow F(A_1) < F(A)$
$\bar{z}_1 > \bar{z} \rightarrow F(\bar{z}_1) < F(\bar{z}), \quad (\bar{z} = v + c)$

and the first statement of (52) is also exhibited in the figure. F is dependent on the film thickness h via Γ_o of (50) and f of (42). But, as shown in figure 3, F is only very weakly dependent on h.

2.3 DISPERSION RELATION

As discussed in 1.2 and 2.2, velocity potential and force balances are approximated only locally and attention is focussed at the point z=0. When equation (7) had been retained in it's full form and a large number of constants c_i had been determined, a higher accuracy could have been achieved. At the present level of approximation, it is sufficient to make the force balance (43) hold at the point z=0 near the crest. This will yield a dispersion relation $c = c(k,A)$. With reference to (16) through (18) the following definitions are introduced :

(53) $\{\{1\}\} = k\eta \operatorname{ctgh}(k\eta+kh)\,(k\eta \operatorname{ctgh}(k\eta+kh)-2) + 4F^2k^2\eta^2((5))^2$

$$-(1-2F)^2k^2\eta^2((6))^2$$

$$\{\{2\}\} = -(1-2F'')^2 + ((3))^2\,4F''^2 + ((4))^2$$

(54) $a = -\frac{1}{2}\varrho\,\{\{1\}\} + \frac{1}{2}\varrho' f^2k^2\eta^2((6))^2\{\{2\}\} + \frac{1}{2}\varrho'\,2f\,k\eta\,((6))\,((4))$

(55) $b = -\varrho v\,\{\{1\}\} + \varrho' Vf^2k^2\eta^2((6))\,\{\{2\}\} + \varrho'(v+v_c)fk\eta\,((6))\,((4)) +$

$$+\varrho'(v_c'-v) + \varrho'(\frac{\theta}{h'})^2(v-v_c') + \varrho' f k\eta((6))\,(\frac{\theta}{h'})^2(v-v_c')\ ((4))$$

$$(56)\quad d = -\frac{1}{2}\varrho v^2\{\{1\}\} + \frac{1}{2}\varrho' v^2((6))f^2k^2\eta^2((6))^2 + \varrho' v v_c' fk\eta((6))\ ((4)) +$$

$$+\frac{1}{2}\varrho'[v_c'^2-v^2 +2(\frac{\theta}{h'})^2(v-v_c')v_c' +2vfk\eta((6))(\frac{\theta}{h'})^2(v-v_c')\ ((4))] +$$

$$+\frac{1}{2}\varrho'\,(\frac{\theta}{h'})^4\,(v-v_c')^2 + \sigma\,\frac{k\eta}{h'(kh'-k\eta)} - \sigma\lambda_+ +$$

$$+\eta''(\cos(kz) = 1)\,\{1 + \eta'(\cos(kz) = 1)^2\}^{-3/2}$$

From (43) the equation

$$(57)\quad ac^2 + bc + d = 0$$

can be derived. In (57) as well as (42) η is given by the equation $kA.\sinh(kh+k\eta)/\sinh(kh) = k\eta$. As stated in 1.1.2 an amplitude dependency has appeared in the dispersion relation. It represents the main non-linear effect of dispersive systems and will be dealt with in full detail in 2.4.3. The dispersion relation given by (57) indicates when a wave is rapidly growing and when it is stable (see 1.2). The former is the case when

$$(58)\quad b^2 < 4ad$$

Our aim is an equation determining stability in a practical form for flow regime prediction. When (53) through (56) are fed into (58), the resulting expression offers no clear constraint on the relation between the velocities v and v_c'. For this the determinant b^2-4ad is further evaluated. From a straightforward but tedious calculation follows:

$$(59)\quad b^2 - 4ad = (v-v_c')^2\,(\frac{\eta}{h'})^2\,(2 - \frac{\eta}{h'})^2\,(k\eta)^2\,\varrho'\{\{9\}\} +$$

$$+ 2\,\sigma\,k^5\,\eta^4\,\{\{3\}\}\,\{\{4\}\}$$

with

$$(60)\quad \{\{0\}\} = \mathrm{ctgh}(kh+k\eta)\,[\mathrm{ctgh}(kh+k\eta) - \frac{2}{k\eta}] + 4F^2((5))^2 - (1 - 2F)^2\,((6))^2$$

$$(61)\quad \{\{9\}\} = \varrho\,\{\{0\}\} + \varrho'\{\frac{1}{(k\eta)^2} + (1 - 2F^*)^2\, f\,((6))^2 +$$

$$- ((3))^2\, 4\, F^{*2}\, f^2((6))^2\}$$

$$(62)\quad \{\{3\}\} = \varrho\,\{\{0\}\} - \varrho'\{ (2f\,((6))\,((3))\,F^*)^2 + [f\,((6))\,((4))]^2 +$$

$$- [\, f\,((6))\,(1 - 2F^*)\,]^2 + 2\, f\,((6))\,((4))\,\}$$

$$(63)\quad \{\{4\}\} = \{k\eta\, kh'\,(kh' - k\eta)\}^{-1} - 2((6))^2\,(1-2F)\,\{1 +$$

$$+ k^2\eta^2((6))^2\,(1-2F)^2\,)^{-3/2}\{\mathrm{ctgh}(kh) - 4F\,\mathrm{ctgh}(2kh)\} +$$

$$+ (k\eta\,\mathrm{ctgh}(kh+k\eta)-1)^{-2}\{1+ 4F^2k^2\eta^2((5))^2(k\eta\,\mathrm{ctgh}(kh+k\eta) +$$

$$- 1)^2\,)^{-3/2}\,\{\,\cosh(kh+k\eta) - \frac{\sinh(kh+k\eta)}{k\eta} +$$

$$+ 4F^2(\mathrm{ctgh}(kh+k\eta)\,((5))^2 + \sinh(kh+k\eta)\,\cosh(kh +$$

$$+ k\eta)/\cosh^2(kh)\,)+4F^2((5))\tanh(kh) +4F^2\frac{1}{\cosh^2(kh)}(\mathrm{ctgh}(kh +$$

$$+ k\eta) + \sinh(kh+k\eta)\,\cosh(kh+k\eta)/(1 - k\eta\,\mathrm{ctgh}(kh+k\eta)\,)\,)\,\}$$

2.4 Stability calculations

2.4.1 Criterion. The liquid film is unstable when

$$(64)\quad (v-v'_c)^2 > \frac{\sigma}{h'\varrho'}\,\mathrm{FACT}$$

with FACT given by

$$(64a)\quad -2\,(kh')^3\,\{\{4\}\}\,\{\{3\}\}/[\,(2 - \frac{k\eta}{kh'})^2\,\{\{9\}\}\,].$$

Since usually $\{\{4\}\} < 0$, equation (64) offers a useful criterion. It can be seen from (64) that surface tension is stabilising, as expected. The form given to (64) and (64a) was inspired by the fact that $\{\{3\}\}/\{\{9\}\} \sim 1$ when ϱ

$\gg \varrho'$, whence it was hoped that FACT would be approximately constant in some, practically relevant circumstances. Resulting dependencies for FACT will be discussed in 2.4.5.

2.4.2 Determination of wave number. FACT will now be calculated as a function of the physical parameters ϱ, ϱ' and R. To this end the most dominant wavenumber k_o is determined from

$$(65)\quad \frac{d}{d\bar{k}}\Big|_{k_o} (k \text{ Im } c) = 0$$

where Im c denotes the imaginary part of c (see section 1.2). For waves with wave number k_o, the opposite of (64) must hold

$$(v - v_c')^2 < \frac{\sigma}{\bar{h}'\varrho'} \text{ FACT}$$

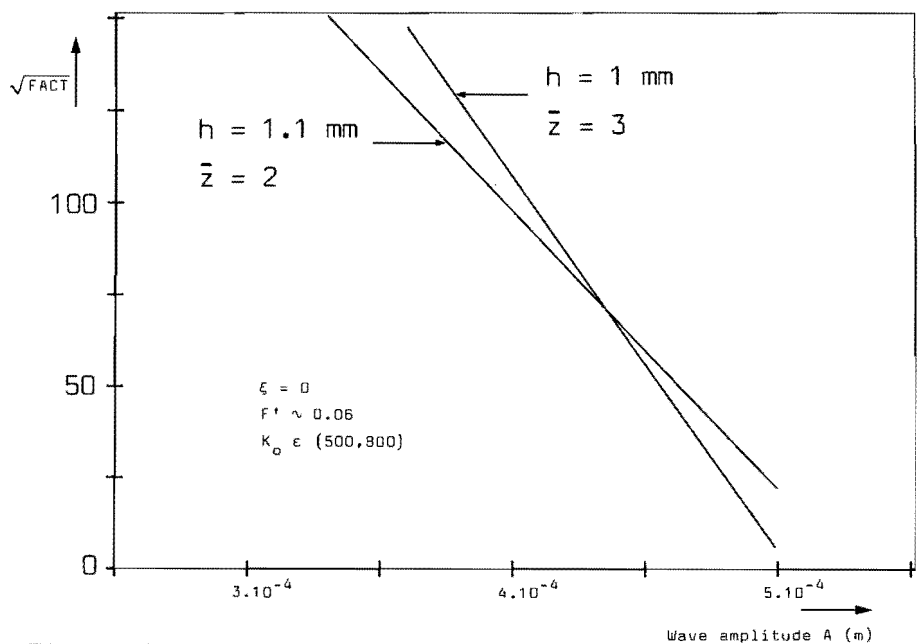

Figure 4
Stability factor versus wave amplitude

whence

$$(66)\quad 2\,\sigma k\,(k\eta)^4\{\{3\}\}\,\{\{4\}\} = -(\xi+1)(v-v_c')^2\,(\frac{\eta}{\bar{h}'})^2(2-\frac{\eta}{\bar{h}'})^2(k\eta)^2\varrho'\ \{\{9\}\}$$

for some dimensionless quantity ξ with :

(67) $-1 < \xi < 0$

Though the exact value of ξ is not known in advance, it is conjectured that ξ is close to zero. It will be demonstrated that results are practically independent of ξ. Expressions are needed like the following ones :

$$((\bar{3})) \overset{\text{def}}{\equiv\equiv\equiv} \frac{d}{d\bar{k}}\Big|_{k_o} ((3)) = 2\,k\theta\,((9)) - 2kh'((3))\,I_o(2kh')/I_1(2kh')$$

$$\{\{\bar{0}\}\} \overset{\text{def}}{\equiv\equiv\equiv} \frac{d}{d\bar{k}}\Big|_{k_o} \{\{0\}\} = (1 - \text{ctgh}^2(kh+k\eta))\,(\text{ctgh}(kh+kh) - \frac{2}{k\eta})\,(kh +$$

$$+ k\eta) + \text{ctgh}(kh+k\eta)\,\{\,(kh+k\eta)\,(1-\text{ctgh}^2(kh+k\eta))+2/(\eta k)\,\} +$$

$$+ 8F^2\,((5))\,((\bar{5})) - (1-2F)^2 2\,((6))\,((\bar{6})) + 8F\,\bar{F}\,((5))^2$$

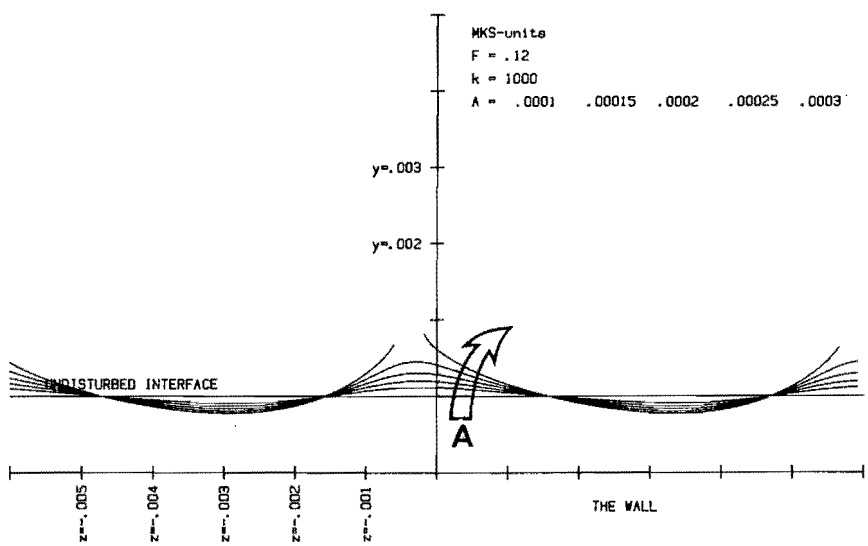

Figure 5

Examples of waves with different amplitudes ($k = 1000$; $F = 0.12$)

with $\bar{F} \overset{\text{def}}{\equiv\equiv\equiv} \frac{d}{d\bar{k}}\Big|_{k_o} F$ etc. Since these calculations are straightforward, but the resulting equations very lengthy, here only one result is presented. One derives from (65) with the aid of (66) and (57):

$$(68)\quad 0 = -\xi\,\{\varrho\, k\eta\{\{\bar{0}\}\} - 2\varrho' f\,\bar{f}\, k\eta\,((6))^2\{\{2\}\} - 2\varrho'\,\bar{f}\,((6))\,((4)) +$$

$$- \varrho' f^2 k\eta[2((6))\,((\bar{6}))\,\{\{2\}\}+((6))^2\{\{\bar{2}\}\}\,]-2\varrho' f[\,((\bar{6}))\,((4)) +$$

$$+ ((6))\,((\bar{4})) - ((6))\,((4))\,]\,\} + \{\,-\tfrac{1}{2}\varrho\, k\eta\,\{\{0\}\} +$$

$$+ \tfrac{1}{2}\,\varrho'\, f^2\, k\eta\,((6))^2\,\{\{2\}\} + \varrho' f\,((6))\,((4))\,\}\,\{-(\xi +$$

$$+ 1)\,\{\{\bar{4}\}\}/\{\{4\}\} - (\xi+1)\,[\,\{\{\bar{3}\}\}\,/\,\{\{3\}\} + 1] + \{\{\bar{9}\}\}/\{\{9\}\}\,\}$$

where it is understood that k stands for k_o in (66) through (68).
For any given set of physical parameters (ϱ, ϱ', σ, R), equation (68) determines k_o and therefore also FACT which is a function of the wave amplitude. As shown in figure 4, obtained for our standard parameter set and R = 0,0195 m, small-amplitude waves are more stable than larger amplitude waves that are affected by internal motions in the core, which in turn are determined

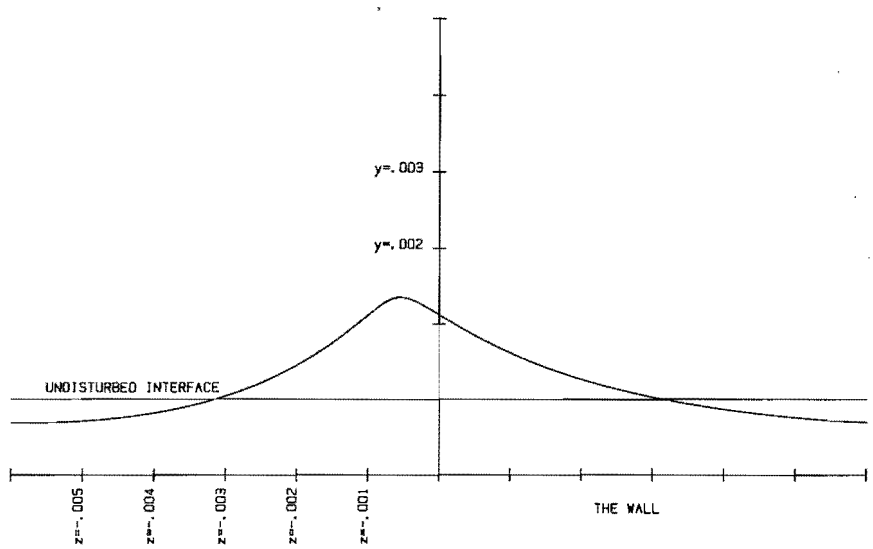

Figure 6

Example of a wave with a critical amplitude (k = 500 ; F = 0.1)

by the upward motion of a gas/vapor plug (see 1.1.1 and 2.2.1). It is also clear from figures 2, 4, 5 and 6 that in order to determine FACT, we need a relationship between A and other physical parameters of interest.

2.4.3 Determination of wave amplitude and wave form. A useful limiting relationship between A and k is offered by the demand that for some z the slope of the wave, as quantified by $\eta'(z)$, becomes very large. It is evident from (14) that, whatever the value of F, this happens at the location z=0 when (20) holds for $k\eta(z=0)$. Equation (20) determines a value for $k\eta(z=0)$ close to 1 for all kh > 0.5. Let $k\eta_{max}$ denote the value of $k\eta$ that is obtained by keeping F.sin(kz) fixed and equating the multiplying factor of η' in the LHS of (14) to zero. The wave amplitude A corresponding to a value for $k\eta_{max}$ can be calculated from:

$$(69)\quad kA = k\eta_{max}\left(1 - \frac{(\,F\sin(kz)\,)^2}{F^2}\right)^{-\frac{1}{2}}\left(\frac{\sinh(kh+k\eta_{max})}{\sinh(kh)} + \right.$$

$$\left. - 2\,(F\sin(kz)\,)\,\frac{\sinh(2kh + 2k\eta_{max})}{\sinh(2kh)}\right)$$

Here $k\eta = k\eta(z)$. As can be seen from figure 7 where numerical solutions for $k\eta_{max}$ are shown, in principle $k\eta_{max}$ may attain a value smaller than 1 for some $z \neq 0$ when $F \neq 0$. However, the minimum value of $k\eta_{max}$ by definition corresponds to the minimum value of kA that can be obtained from (69) by varying kz but keeping both F and kh fixed. Take for instance kh = 10; when F = 0.3, the minimum value for kA is about 2.4, in shorthand $kA(F=0.3) \approx 2.4$. With the same meaning :

F	kA
0.5	2.31
0.4	2.33
0.2	2.57
0	2.72

For each F, the minimum value of $k\eta_{max}$ is close to 0.75. From these observations a limiting value for $k\eta$ is concluded to lay in the interval [0.75,1], while $k\eta_{lim}(z=0)$ is close to 1; only for long wavelength's ($kh<\frac{1}{2}$) may deviations occur.

Some experimental evidence exists too for the existence of a relationship between the wave number and the (maximum) wave amplitude shortly before the break-up of the wave. Although only from experiments on horizontal

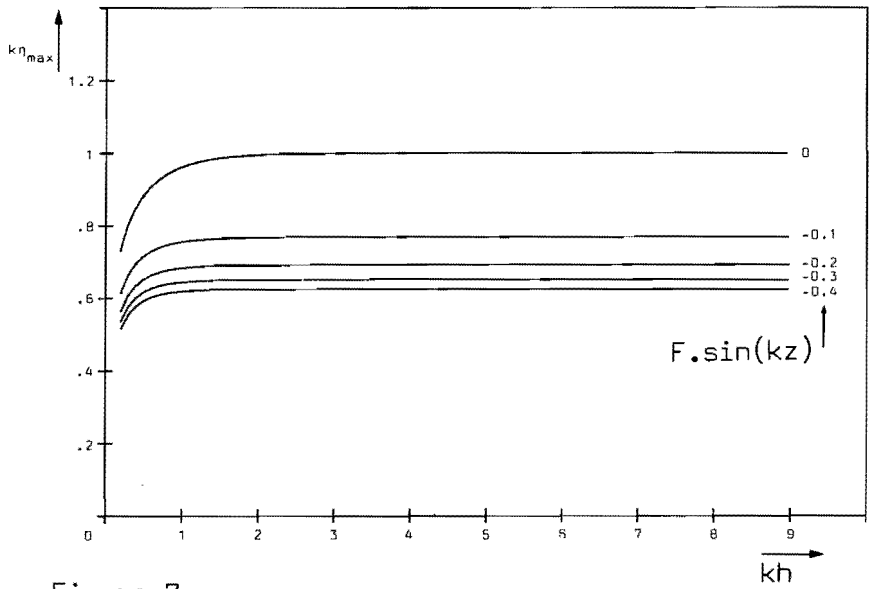

Figure 7

Determination of $k\eta_{max}$

air/water flows, Kordyban and Ranov (1970) reported a value of 0.9 for $k\eta_{lim}$. Note that by comparing figures 2 and 5, one is already tempted to believe that a relationship exists between k and $k\eta_{max}$. These results are to be compared with the $k\eta_{max} \approx 0.74$ reported in 1.1.1 and the lower bound on $k\eta$ with value 0.57 as discussed in 1.1.2. The limiting values for both cases are strikingly close, especially if one takes into account that the dominant forces and the derivations involved are quite different. This observation and the physical arguments given in 1.1 are the reasons for selecting values for $k\eta$ in the interval [0.5, 1].

So in the quest for FACT, or rather √FACT (see (64)), either a value for A to each wave number has to be selected in such a way that $k\eta_{max}(z=0) \in [0.5, 1]$, or else $k\eta(z=0)$ should be given a definite value before solving (68) and other equations. The last option has been chosen, though it changes all equations with a differentiation with respect to k in it. After this modification, FACT has been calculated numerically for several $k\eta_{max}(z=0)$ with our standard set of parameters and R = 0.0195 m. Some results are gathered in figure 8. It clearly shows that a dependency on the parameter $k\eta_{max}$ is only introduced via the dependency on the parameter F. Also other

values in the interval [0.5, 1] have been examined, but they do not lead to notable differences. The influence of the parameter $\bar{z}$ will be discussed presently. Since from (49) and (50) F can only be estimated ($\bar{z}$ = v+c is unknown in advance, see also 1.2) and, according to the results discussed above, the equality $k\eta_{max}(z=0)=1$ overpredicts kA with an error of at the most 10%, the parameter $k\eta_{max}(z=0)$ is kept fixed at the value 1 henceforth. For the k_o calculated with (68) the inequality $k_o h > \frac{1}{2}$ proved to be correct. From the combination of (52) and (51), it is clear that $|\bar{z}|$ can not be chosen arbitrarily small, while too large a value of $|\bar{z}|$ would make F vanish altogether. Figure 8, which shows results for $\bar{z}$ = 2 and $\bar{z}$ = 3, demonstrates that $\sqrt{FACT}$ is influenced by the choice of $\bar{z}$ in the estimation of F, but not much. This influence can be ignored for high values of $\bar{z}$ of course. Since

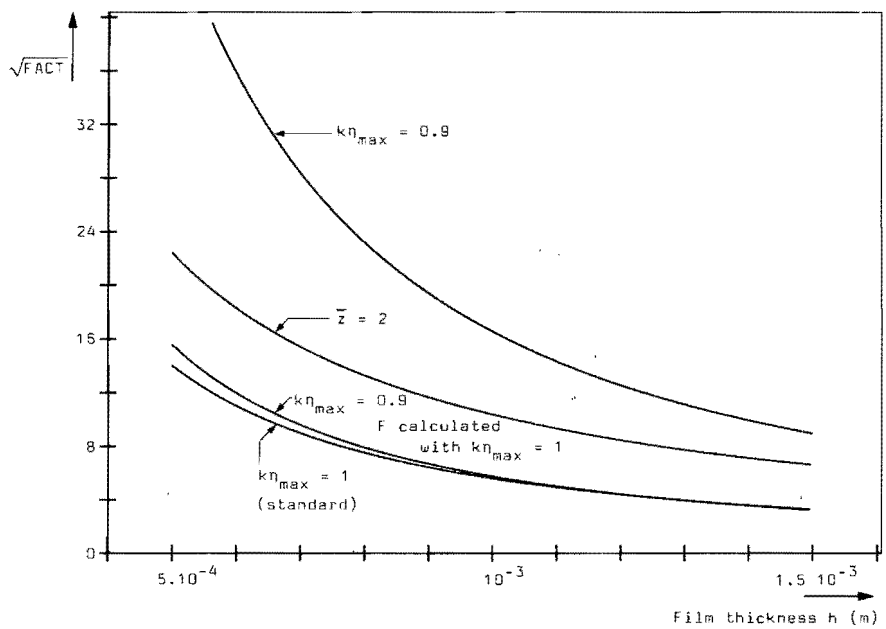

Figure 8

Stability curves ; dependency on $k\eta_{max}$ and z

the value of F (and hence $\bar{z}$) is closely connected to the waveform, F is determined ultimately by the flow states that are most commonly observed in experiments (see also 1.2). As can be seen from figure 8, an increasing accomodation of the wave to its environment (the possible cause of disturbances), as reflected by an increasing value of F, results in a stabilisation of the wave. This feature is what one expects. If a large amount of unnecessary energy dissipation (break-up of the wave) can be avoided by a form of accommodation that involves less energy dissipation,

this accomodation will take place. Since flow development is not studied explicitly (see 1.2), the value of $\bar{z}$ has been fixed at 3. As stated in 1.2, no attempts have been made to readjust $\bar{z}$ after computation of c from $\frac{-b}{2a}$ (see (54) and (55)) for example, but when $\varrho \gg \varrho'$ this expression for c suggests a low value for $\bar{z}$, limited though as it is by (51).

2.4.4 Dependency on ξ. From experimental observations it appears that wave numbers of interest must occur in the interval given by

(70) $k\varepsilon$ [100, 1500]

(see Portalski (1963) for example). Now (70) and (51) are used to compute k_o

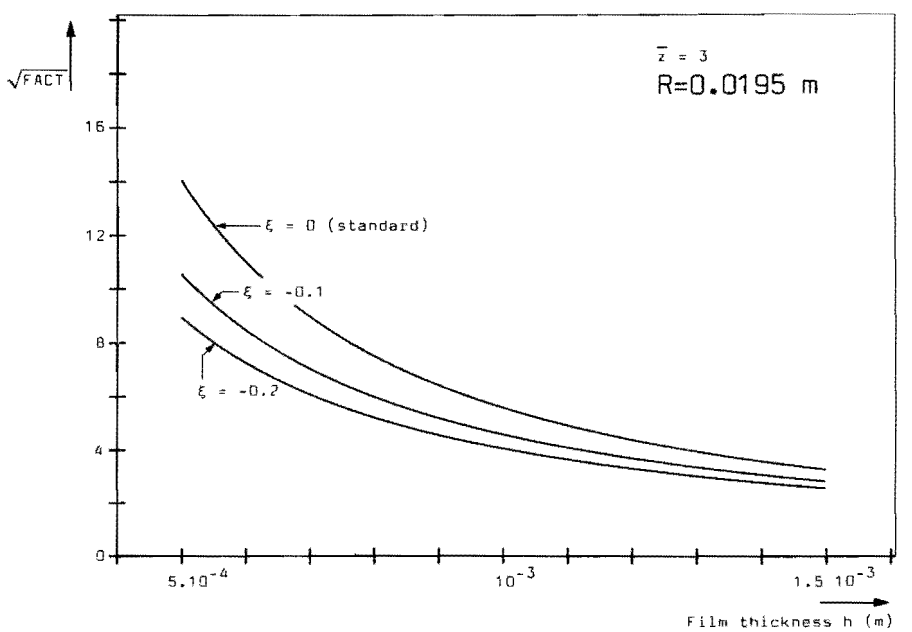

Figure 9

Stability curves ; dependency on ξ

numerically from (68), and for example, figure 9 is obtained. This figure shows how FACT, obtained from (64a) with an additional factor of $(1+\xi)^{-1}$ in the RHS, decreases with increasing $|\xi|$. Although it is known that $\xi \neq 0$ for the wave with the highest amplification rate, we shall make $\xi = 0$ henceforth because figure 9 shows that it does not make much difference anyway, and

because there are no indications as to an appropriate value for ξ whatsoever. Because of this choice :

(71) $\sqrt{FACT}$ is slightly overpredicted.

Figures 8 through to 11 exhibit the same trend. Stability increases with decreasing film thickness. This is evident, since on a thin liquid film only waves with relatively small amplitudes will occur; these smaller amplitude waves are less affected by internal circulation. For our standard parameter set (ρ=1000, ρ'=1.18 and σ=0.073, MKS units) and R=0.0195 m the results could be correlated very well (total relative error less than $\pm$ 0.3 %) by

(72) $\sqrt{FACT} = 119.088\ (h.10^4)^{-1.329}$

with h in meters.

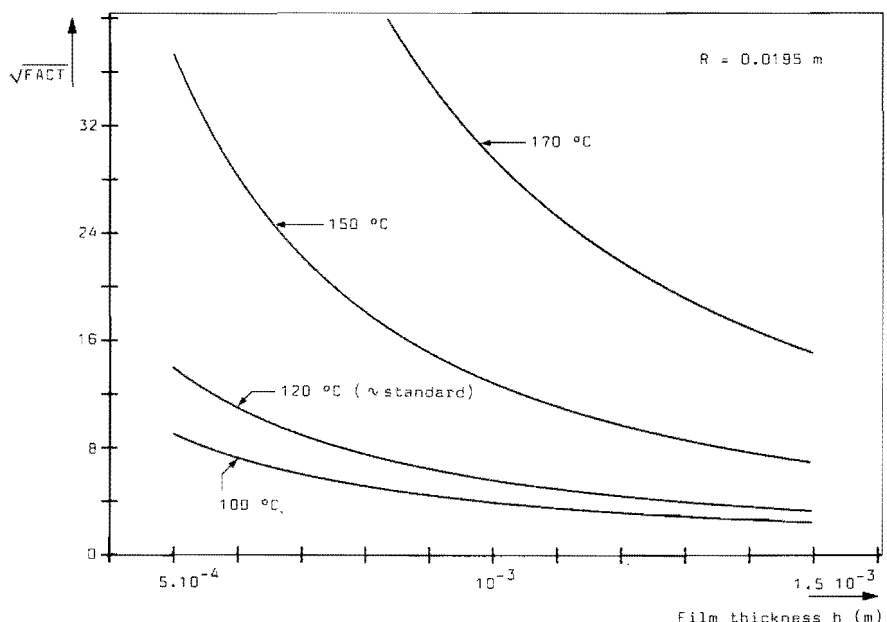

Figure 10

Stability curves ; dependency on (saturation) temperature

2.4.5 Dependency on temperature and tube radius. By selecting values for ρ, ρ' and σ corresponding to saturation temperatures, the influence of system pressure on steam-water systems was studied. Some results have been gathered

in figure 10. Since for T_{sat} = 120°C, ϱ = 940.167, ϱ' = 1.217 and σ = 0.0549 (MKS units), the curve for T_{sat} = 120°C is very close to the curve for our standard parameter set, which corresponds to an air-water system at room temperature. The results have been correlated by

$$(73)\quad \sqrt{FACT} = 0.68 \exp(0.0439\ T)\ (h.10^4)^{-(0.539 + 0.0066\ T)}$$

with h in meters, T in °C and R = 0.0195 m. The relative error of the exponential factor amounts to 11 %. The error induced by the functional exponent of h 1 %.
Multiplying $\sqrt{FACT}$ by $\sqrt{\frac{\sigma}{\varrho}\tau}$ (0.314 for T=100°C and 0.104 for T=170°C), we can find the effective dependence of stability on temperature (see (64)). Typical values for $\sqrt{FACT}.\sqrt{\frac{\sigma}{\varrho}\tau}$, obtained for h=1 mm, are: 1.23 (T=100°C) and 3.07 (T=170°C). So at higher temperatures liquid films are more stable, which is due to decreasing differences between the two phases water and

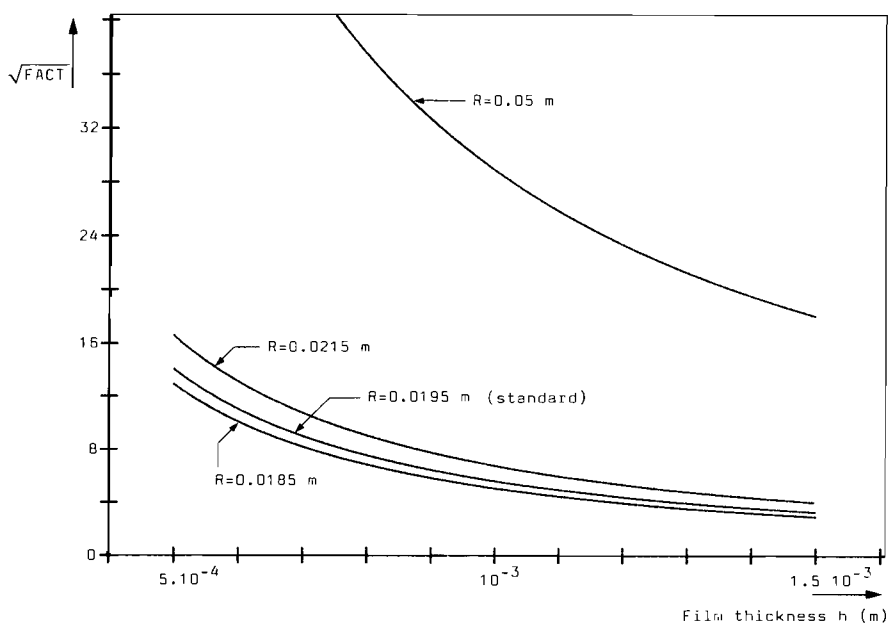

Figure 11

Stability curves ; dependency on tube radius

vapor. A study of the separate effects of surface tension and densities on $\sqrt{FACT}.\sqrt{\frac{\sigma}{\varrho}\tau}$ reveals that this stability term increases with increasing σ or decreasing $|\varrho-\varrho'|$. Stability is increased when the tube radius is increased. This too is evident, since for larger tubes, gradients in the $\hat{r}$-direction of

the undisturbed core velocity are less pronounced, which causes waves to be less easily affected by the internal motions (see figure 11). Again we have to take notice of the definition of FACT, and some typical values for the relevant expression $(R-h)^{-0.5}./FACT$, obtained for h=1 mm, are: 38.17 (R=0.0185 m) and 129.07 (R=0.05 m).
The results have been correlated (relative error ± 3 %) by

$$(74)\quad /FACT = 49.51\ (100\ R)^{1.322}\ (10^4 h)^{g(R)}$$

with R and h in meters, and with the function g being given by (relative error ± 2 %)

$$g(R) = -1.468\ (100\ R)^{-0.147}$$

With a relative error of ± 12% /FACT can be computed from the following correlation:

$$/FACT = 0.281\ (100\ R)^{1.322}\ \exp(0.044\ T)\ (10^4\ h)^{s(R,T)}$$

with $s(R,T) = -(100\ R)^{-0.147}\ (0.5946 + 0.00728\ T)$

T in ^{o}C, R and h in m. For application at air-water systems the value $120^{o}C$ for T can be used, as noted before.

3 FLOW REGIME PREDICTION

3.1 Plug flow and the onset of churn flow

When the liquid film of a plug becomes unstable due to the presence of exponentially growing finite amplitude waves, we no longer speak of plug flow, but rather of churn flow (see 1.1). As will be demonstrated in 3.3, this either occurs in the entrance region of plug flow or when the superficial velocities surpass certain boundary values. If we are to predict the flow pattern present using (64) and (72) with given superficial velocities (and tube diameter D and temperature T), we have to calculate v and v'_c. A calculation scheme for this purpuse will now be presented. It will enable us, in 3.2, to compare our findings with experimental data and other predictions, most commonly presented in so-called flow regime maps.

Let U'_s denote the superficial air/vapor velocity, ε the geometrically and time averaged void fraction, u_s the superficial water velocity, L_p the nose-to-tail length of a plug or Taylor bubble and L_{SL} the tail-no-tose length of the water slug behind a Taylor bubble.

From a simple geometrical consideration we have the approximation :

$$(75) \quad \varepsilon = \frac{L_p}{L_p+L_{SL}} \left(1 - \frac{2h}{D}\right)^2$$

On the other hand the void fraction can readily be calculated from the well-established correlation:

$$(76) \quad \varepsilon = u'_s / v'$$

The mean gas/vapor velocity v' will be used to estimate v'_c and follows from, (see Moissis and Griffith, 1962) :

$$(77) \quad v' = 1.2\ (u'_s+u_s) + \{\ 0.35 + 2.8 \exp(-1.06\ \frac{L_{SL}}{D})\ \}.\sqrt{gD(\varrho-\varrho')/\varrho}$$

According to Akagawa and Sakaguchi (1966), the factor 1.2 on the R.H.S. of (77) amounts to 1.3 when bubbles appear in the liquid slug. For similar circumstances the value 1.29 has been reported by Fernandes (1981). The

constant 0.35 in the R.H.S. of (77) is a result firmly established for the rise velocity of Taylor bubbles through stagnant liquids. Stewart and Davidson (1967) summarized experiments to determine this constant, and the paper of Collins et al. (1978) provides strong theoretical support.

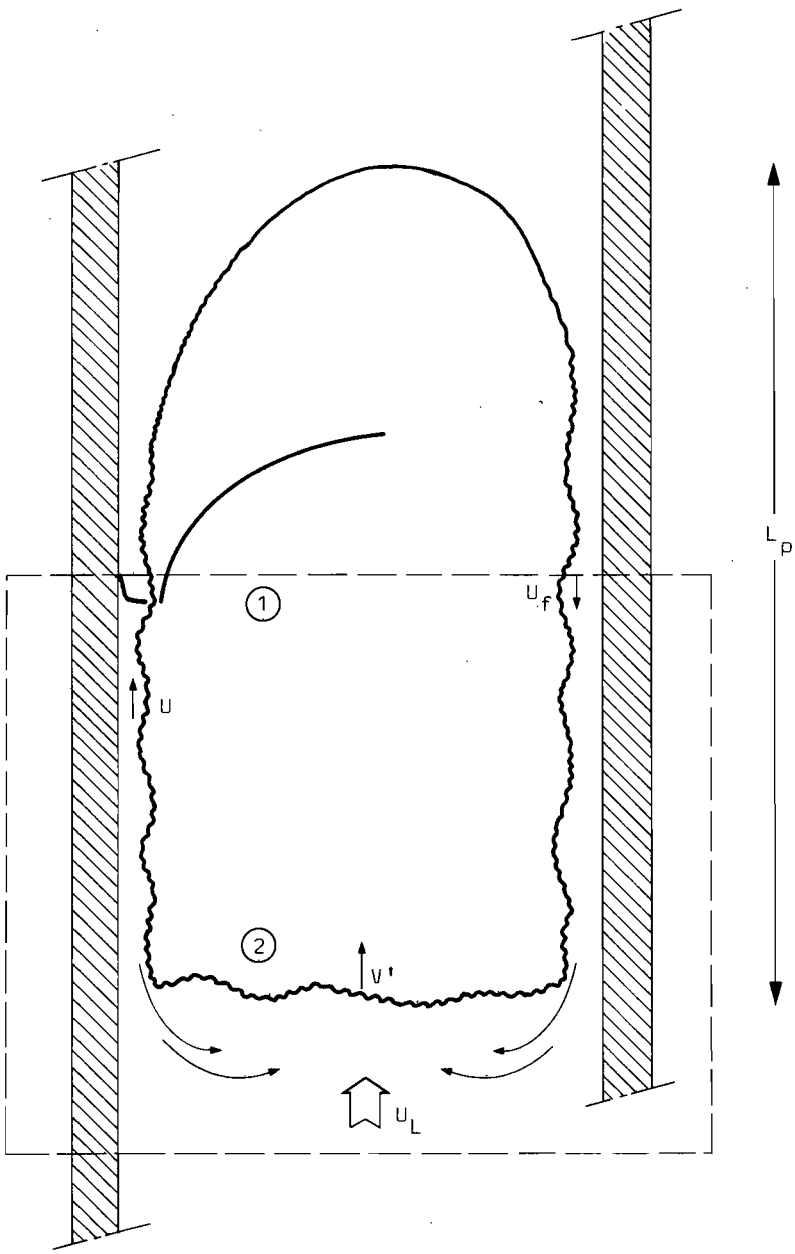

Figure 12
Characteristics of plug flow

We define U_L as the mean liquid velocity inbetween two Taylor bubbles (see also figure 12):

$$U_L = \frac{1}{\pi R^2} \int_0^R dr\ 2\pi r\ U_L(r)$$

Since the instantaneous liquid velocity U(t) follows from

$$(78)\quad U(t)\ (1 - \varepsilon(t))\ \pi R^2 = (U_s' + U_s) - \varepsilon(t)\ \pi R^2\ U'(t)$$

we have $U_L = U_s' + U_s$ when the total volumetric flowrate is constant. Note that quantities are time-dependent, which is typical for strongly intermittent flows.

In the frame of reference moving upward at a velocity v' with respect to the laboratory frame, we obtain by applying continuity of mass to the box shown in figure 12:

$$(u_f + v')\ \pi\ (R^2 - (R-h)^2) = (v' - U_L)\pi\ R^2$$

and by considering the core motions of the Taylor bubble at cross-section 1:

$$\int_0^{R-h} dr\ 2\pi r\ \rho'\ (U'(r) - v') = 0.$$

Hence, using the former equation :

$$(79)\quad u_f = [4h\ (D-h)]^{-1}\ \{\ v'(D-2h)^2 - D^2(U_s + U_s')\ \}$$

and, combining the latter equation for the core motions with (33) with c=0 :

$$(80)\quad 2v' = v + v_c'$$

where v denotes the undisturbed velocity of the liquid surface, and is approximately given by $-|u_f|$. In order to evaluate (72), we have to calculate h; in appendix 1 following expression is derived:

$$(81)\quad h = \sqrt{\left\{ \left[\frac{D-h}{D-2h}\right].\left[\frac{K_1 \nu\, u_f}{g(1-\varrho'/\varrho)}\right] \right\}}$$

with K_1 varying between 2.4 and 3. Let $\gamma = D^{-1}\sqrt{\left\{ \left[\frac{D-h}{D-2h}\right].\left[\frac{K_1\,\nu}{g(1-\varrho'/\varrho)}\right] \right\}}$ be the defining equation for γ. A typical value for γ is 0.013 for D=0.039 m and air/water at room temperature. The parameter γ will be treated as a constant, but it will be shown in 3.2 that the results are not influenced by the uncertainty in K_1 or the fact that γ is not really a constant due to the appearance of h in its definition. We also assume L_{SL} to have a constant value but shall dwell on L_{SL} further in 3.3.
Substituting (81) in (79) one finds that

$$(82)\quad o^4 + po^2 + qo + r = 0$$

with $o = \sqrt{u_f} - 1/(4\gamma)$
$p = v' - 3/(8\gamma^2)$
$q = -1/(8\gamma^3) - v'/(2\gamma)$
$r = -3\gamma^{-4}/16^2 - 3v'\,\gamma^{-2}/16 - (U_s + U_s' - v')/(4\gamma^2)$

By reducing (82) to a cubic equation in the standard way, it can be solved exactly or else, for instance, Newton's algorithm can be used to solve (82) numerically.
The total calculation procedure for the determination of h and the flow pattern present is as follows:

A. Take values for U_s and U_s'
B. Take $L_{SL} = 6D$. As to be discussed in 3.3 other values of L_{SL} yield no information relevant to flow regime prediction
C. Calculate v' from (77)
D. Calculate u_f by solving (82)
E. Calculate h from (81)
   Now ε and L_p follow from (76) and $L_p = L_{SL}\left\{ \varepsilon^{-1}(1-\frac{2h}{D})^2 - 1 \right\}^{-1}$
F. Calculate $\sqrt{FACT}$ from (72) for instance and check the inequality
   $|v-v_c'| < \sqrt{FACT}.\sqrt{\frac{\sigma}{h'\varrho'}}$

According to (80), the maximum value of $|v-v_c'|$ in the Taylor bubble is $2(u_f+v')$. Near the bottom of the plug (at cross-section 2, see figure 12)

gas/vapor entrainment into the liquid slug is caused by the falling liquid film (see for instance Fernandes, 1981, and Jones and Zuber, 1975). The bubble content is supplied via the nose of the plug and exploding bubbles in the water surface (see 1.1.2). For this, the value of $|v-v_c'|$ near the bottom of the plug is estimated to be close to $(u_f + v')$. Accounting for the fact, that the relative velocity $|v-v_c'|$ is not critically high everywhere, we use the sort-of averaged value $1.5(u_f + v')$ for it. Although the results of course depend on the value of $|v-v_c'|$ of course, the only way to improve on this averaging procedure is to determine exactly when a wave starts increasing in amplitude, to study wave development and to predict more accurately the undisturbed core velocity profile and how it depends on z. For the latter it is necessary to determine exactly how much gas/vapor is captured and entrained in the liquid slug. This alternative approach and its drawbacks have been discussed at length in 1.1.3 and are clearly beyond the scope of the present investigation.

3.2 Comparison with experiments

When results of the stability analysis of chapter 2 are used in the calculation scheme of 3.1, the plug-churn flow regime transition can be predicted. In this section predictions made in this way are compared with experiments done by the author and with experimental and theoretical investigations found in the literature. The conclusions of the current section depend on the prediction scheme of 3.1, but of course any other scheme can be selected to test the stability analysis presented in chapter 2.

Predictions for an air-water system at room temperature are compared with experimental observations and predictions of, for example, Taitel, Bornea and Dukler (1980) in figure 13. When the superficial water velocity is larger than about 1 m/s, flow regimes such as bubble flow may occur, which makes this part of the figure irrelevant. A inner tube diameter of 3.9 cm has been chosen because of the fact that measurements with the Flow Pattern Indicator (see van der Geld, 1984) are available for this case. These new experimental results are also exhibited in figure 13. It is interesting to note that for higher liquid velocities, experimental observations and the theoretical transgression curve show opposite trents. From (77) and (79) it

can be seen that, according to the prediction scheme of 3.1, the transition is largely determined by the total volumetric flow rate U_s+U_s' .

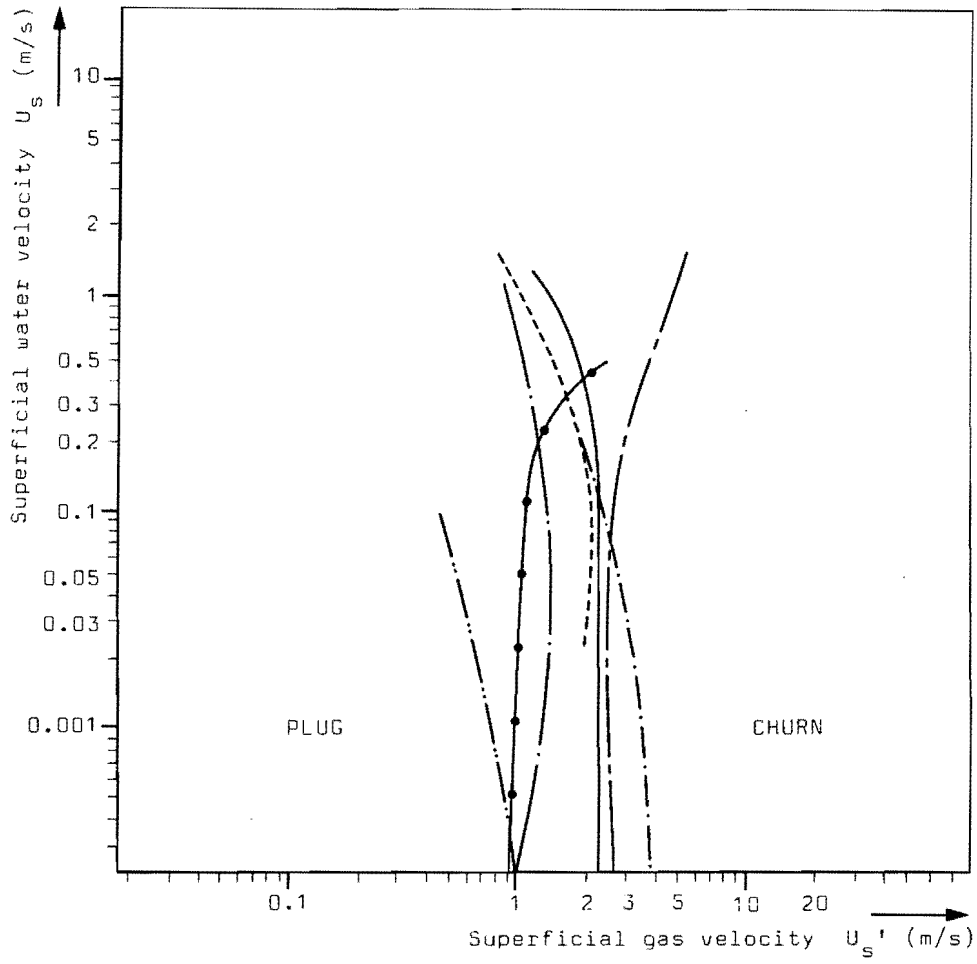

Figure 13
Comparison with experiments in flow pattern map

This explains the trend of the curve representing the theoretical predictions. Most probably the discrepancy with the trend of the curve

representing Flow Pattern Indicator results is due to difficulties in distinguishing experimentally whether a liquid film is stable or not (see in 1.1.1, the part dealing with foaming).

In order to study the dependency of the predictions on calculations of the liquid film thickness via the parameter K_1 (see 3.1), several different values for γ have been put into these calculations. It turned out that a variation of 10 % in the value of γ resulted in a variation of 4 % at the most in the value of transitional superficial gas/vapor velocities. Such small differences are neglectable on the logarithmic scales of the flow pattern map. The theoretical curve drawn in figure 13 was calculated with γ = 0.013 and with the aid of (72). It should be noted that the relative unimportance of the parameter K_1 is not fortuitous, but is established by the explicit form of the functional dependence on h of $\sqrt{FACT}$. For if $\sqrt{FACT}$ is kept constant in the calculations, the flow regime predictions turn out to be very dependent on the value of K_1 (or γ). This is in sheer contrast with the results obtained using equation (72). This observation gives confidence in the results of the stability analysis of chapter 2 and especially in the combination of the resulting equation (72) with the calculation scheme of 3.1.

Not shown in figure 13 are predictions of the present theory for the case D=2.5 cm. Critical superficial gas/vapor velocities are found to be $\pm$ 5 % higher for D=2.5 cm than corresponding ones for D=3.9 cm. Since conclusions based on the functional expression for $\sqrt{FACT}$ alone were different (see 2.4.5) the factor u_f+v' used in (64) increases when D increases. That this observation is correct can also be seen directly from (77) and (79). Again, resulting differences between transgression curves corresponding to these two tube diameters are hardly discernable on a flow pattern map with logarithmic scales. However, the prediction that transition gas velocities for large-diameter tubes are lower lends itself to experimental validation. One of Haberstroh and Griffith's conclusions (1969) for the transition of churn (or semi-annular flow as they call it) to annular flow can be quoted : " There is an uncorrelated diameter effect which tends to depress the transition gas velocity for large-diameter tubes at low pressure". Since the transition for which the above statement is valid is also related to wave phenomena, the Haberstroh and Griffith conclusion may be a first indication that the above prediction regarding the dependence of the plug-churn flow

regime transition on the tube diameter is correct. No explicit experimental study on this topic is known to the author. The theoretical finding that the transgression curve for D=2.5 cm is close to the one for D=3.9 cm supports the implicit assumption that is tacitly made by comparing experimental data for different tube diameters in one and the same flow pattern map (see Taitel, Bornea and Dukler, 1980, for instance).

The author would like to compare the theoretical predictions regarding dependencies on temperature or surface tension with experimental data concerning the plug-churn flow pattern transition. With the current state of knowledge, such a comparison is not meaningful. Not only are measurements at high temperatures scarce, but also different flow regime definitions are employed (see Bergles and Suo (1966) for instance). Measurements at room temperature that would make it possible to compare the equipment and flow pattern definitions used with those of others are omitted. For these reasons the author is currently performing experiments at high temperatures, which will be desrcibed elsewhere.

Figure 13 shows that there is good agreement between predictions made with (72) and the calculation scheme of 3.1 and experimental observations. The spread in the results may be due to the occurrence of surface-active agents, the suppression of temperature and diameter effects and the use of different flow regime definitions (See also 1.1). Since some approximations are involved in the present treatment (see (71) for example), it can be recommended that the constant 49.51 in (74) be adjusted to the calculation procedure and flow regime delineation that is adopted for reference measurements at room temperature. To predict flow regime transitions for other circumstances (e.g. temperatures, tube diameters) than for the one for which reference measurements are available, one subsequently only has to apply the adjusted formulae of 2.4.5 and the calculation procedure that was earlier adopted. In this way allowances are made for other calculation procedures than the one of 3.1 and other flow pattern definitions. However, if no other flow regime delineation or calculation scheme is available, the combination of sections 3.1 and 2.4.5 is recommended to determine the transition from plug flow to churn flow in vertical tubes.

3.3 Complementary with the entry length theory

Taitel, Bornea and Dukler (1980), for example, attributed the slug-churn flow regime transition to entry region behaviour. They proposed calculating an entry length l_E from :

$$l_E/D = 40.6 \{ (u_s + u'_s)/ [gD]^{0.5} + 0.22 \}$$

Note that velocities enter only via the total volumetric flow rate, which was also approximately true in 3.1 as discussed in 3.2. When the location where observations are made is within a distance l_E from the gas-inlet churn flow should be observed. If no other alternatives are involved, slug flow should be observed at other points, though the entry length might cover the entire tube. The qualitative picture is probably correct for adiabatic flows. When the vapor pockets in developing plug flow are small they are unstable. Liquid slugs inbetween them fall back and merge with slugs coming from below. This goes on until a more or less stable configuration has been formed. Liquid slug lengths are then reported as large as $\pm$ 8 or $\pm$ 16 tube diameters. In the current section, it will be demonstrated how this entry length approach fits in with the stability theory developed in this paper. It will also be argued that plug flow evolves into churn flow in evaporator tubes if enough heat is added for the total volumetric flow rate to surpass a certain critical value. When this flow rate is kept approximately constant on the other hand, there may exist an entrance region in which churn flow which is present there evolves into plug flow.

The following predictions are obtained with the aid of equation (72) by using values for L_{SL} as indicated in the table at step B of the calculations procedure of 3.1. When churn flow is indicated in the table, the supposed plug is not present and, for instance, L_p and h represent only fictive quantities. These cases correspond to circumstances in which vague and bubbly void concentrations are discernable in the two-phase mixture in which a stable liquid film may develop only after recombination with other such would-be plugs. For D = 3.9 cm, U_s = 0.1 m/s, and U'_s = 1.9 m/s :

L_{SL}	L_p	h	u_f	Type
1	8	1.28	6.4	churn
2	24	1.1	4.7	churn
3	43	1.02	4.1	churn
4	62	0.99	3.8	plug
5	79	0.98	3.7	plug
6	96	0.98	3.7	plug
7	112	0.98	3.7	plug
D	cm	mm	m/s	-

As can be seen from the table, would-be plugs are smaller than the vapor pockets of the stable configurations, plugs. These small and unstable void concentrations only occur near the gas-inlet and hence indicate an entrance region. The table shows that the choice of the value for L_s is important for flow regime predictions. The closure relation offered by B in the calculation scheme of 3.1 hides the entry length effect. Another example for D=3.9 cm; U_s = 1 m/s, U_s' = 1.3 m/s :

L_{SL}	L_p	h	u_f	Type
1	3	1.29	6.4	churn
2	7	1.11	4.8	churn
3	11	1.04	4.2	churn
4	14	1.01	4	churn
5	18	1	3.9	churn
6	22	0.99	3.9	plug
7	26	0.94	3.8	plug
D	cm	mm	m/s	-

Usually no new results are obtained for $L_s > 6D$. The superficial velocities selected for the above examples correspond to points in figure 13 that are close to the theoretical transition curve. When a pair of superficial

velocities is selected that does not correspond to a point close to this curve, normally the type of flow is correctly given by a prediction made with L_s = 3D. When this is the case, the entrance region is small and can be ignored in most practical circumstances. For these reasons a critical value of 6D could safely be selected in 3.1. As a consequence of the fixation of the value of L_{SL} in 3.1, the theoretical transition curve can only be seen as an idealisation of the transition band that is actually present. Each point of this band corresponds to a certain location of observation.

If plug flow appears in an evaporator tube with an approximately homogeneous heat supply, churn flow may occur in some downstream region where the total volumetric flow rate has grown too large. Then churn flow is created in the upper part of the tube, and not in the lower part as is the case in common isothermal gas-liquid testsituations. This observation has raised discussions (e.g. Nancy 1983, I.U.T.A.M. symposium "Measurement techniques in gas-liquid two-phase flows") whether plug flow progressively alters into churn flow or the other way around. Obviously both views are correct. Though churn flow is created by velocity differences that are too large, the mechanisms that cause these velocity differences can be different.

4 CONCLUSIONS

The following criterion for the onset of churn flow in vertical, circular ducts has been derived theoretically :

$$|v-v'_c| > 0.281\ [100\ R]^{1.322} \exp(0.044\ T)\ [10^4 h]^s \sqrt{\left\{ \frac{\sigma}{\varrho'} \frac{1}{(R-h)} \right\}}$$

with $s = -(100\ R)^{-0.147}(0.5946 + 0.00728\ T)$; R denotes the radius of the tube (m), v'_c the vapor velocity (m/s) at the centre of the tube, h the thickness (m) and v the mean velocity (m/s) of the water film around the vapor plug that is supposedly present. The surface tension σ (N/m) and the vapor mass density ϱ' (kg/m^3) have to be evaluated at the temperature T (^oC). Due to the variance introduced by correlating computational results the uncertainty of the RHS after evaluation of the functional expression on the RHS for a certain temperature and tube radius can amount to 12 % (see 2.4.5).

Transition gas velocities seem to be only moderately dependent on the tube radius. An uncorrelated diameter effect has been derived which depresses the transition gas velocity for large-diameter tubes.

Stability of the liquid film in a plug increases with increasing temperature, increasing surface tension or decreasing mass density difference $|\varrho - \varrho'|$. The temperature of the flow is considered to vary only gradually on a scale of $\pm$ 6 tube diameters. The main idea of the present analysis is, that plug-churn flow pattern transition is caused by film instability governed by a non-linear dispersive interaction with the vapor flow, in which a circulation is present. So a temperature effect has been derived, that depresses the transition superficial vapor velocity for low temperatures.

The functional dependence of the RHS on the film thickness h has been shown to be vital for the prediction of the flow regime present. The explicit form of this functional relationship more or less compensates the uncertainty in theoretical predictions of the film thickness (see 3.2).

For gas-liquid systems of any kind at room temperature, the use of equations (72) or (74) - relative error less than $\pm$ 3 % - is recommended. By repeating the complete stability calculation of chapter 2 for a certain two-phase

flow, temperature and tube radius, other criteria can be derived and the relative error can be decreased to less than 1 %.

A calculation procedure has been put forward in 3.1 that can be combined with one of the correlations mentioned above to predict the flow pattern present from a given set of superficial velocities. Application to air-water systems with the aid of (72) has been shown to yield predictions that agree well with experimental observations.

The theory predicts an entry length region which makes the transition curve in a flow pattern map an idealisation of the transition band that is actually present. So it has been demonstrated that entry length theories are complementary to the stability theory presented.

Further experimental work is necessary in order to test all the predictions in an unambiguous way.

APPENDIX

The thickness of a falling film in circular tubes

Let $R_1 = R-h$. When, along with acceleration forces, friction forces on the surface of the film are neglected, a force-balance on the cylindrical part of the liquid film within a radial distance r from the center of the tube yields

$$\tau(r)\ 2\pi\ r = \varrho\ g\ \pi\ (r^2-R_1^2) \qquad (A-1)$$

with :

$$\tau(r) = -\mu\ \frac{\partial u}{\partial r} \qquad (A-2)$$

Here μ includes turbulent viscosity. In 2.1.1 equation (A-1) has been derived in another way, see equation (6). Let $a = -\varrho g/2\mu$. Integrating from the wall, where velocities equal zero, one gets

$$u(r)= -\ 0.5a\ (R^2-r^2) + a\ R_1^2\ \ln\ (\frac{R}{r}) \qquad (A-3)$$

Note that the second term arises because of the assumption $\tau(R_1) = 0$. The next step is to calculate the total mass flux $\dot{m}$:

$$\dot{m} = 2\ \pi\ \varrho\ a\ R_1^2 \int_{R_1}^{R} r\ \ln(\frac{R}{r})\ dr - \pi\ \varrho a(\ R^2(R^2-R_1^2)/2 - (R^4-R_1^4)/4\ ) \qquad (A-4)$$

The first expression on the R.H.S. is evaluated by means of partial integration :

$$-\dot{m} = \pi\varrho a[R^2(R^2-R_1^2)/2 - (R^4-R_1^4)/4 - R_1^2(R_1^2\ \ln(\frac{R_1}{R}) + R^2/2 - R_1^2/2)\ ] \qquad (A-5)$$

Let $\varphi = \delta/R$, whence $R_1/R = 1-\varphi$. Because $\varphi<1$, one obtains upon expanding $\ln(1-\varphi)$:

$$\frac{\dot{m}}{\pi \rho a R^4} = 4\varphi^3/3 - 4\varphi^4/3 + \ldots \qquad \text{(A-6)}$$

Now

$$\varphi^3 (1-\varphi) \approx \frac{3 \nu}{2\pi R^4} \frac{\dot{m}}{\rho g} \qquad \text{(A-7)}$$

When φ^4 would be neglectable, one could write $\dot{m} = \rho u_f 2\pi R \delta$ and after introduction of the Reynolds number $R_e = u_f \delta / \nu$, a well-known Nusselt-formula would be derived. With $\dot{m} = \rho U \pi (R^2 - R_1^2)$ we obtain from (A-6) :

$$u_f = \frac{g}{2\nu} \frac{R^2}{\varphi(2-\varphi)} \frac{4}{3} (\varphi^3 - \varphi^4 + \ldots) \qquad \text{(A-8)}$$

$$\delta = \sqrt{\left[\left(\frac{D-\delta}{D-2\delta}\right) \left(\frac{3\nu u_f}{g}\right)\right]} \qquad \text{(A-9)}$$

As compared to the Nusselt formula the correction parameter

$$K_2 = \sqrt{\left\{\frac{D-\delta}{D-2\delta}\right\}} \qquad \text{(A-10)}$$

is introduced, in which $D = 2R$. Obviously, K_2 comes into view when the thickness of the film is no longer small as compared to the tube-radius. This may be the case in smaller bore tubes when not only wall-friction and viscosity have to cope with gravity. It is therefore appropriate to take into account effects due to interfacial shear stress too. Let

$$\delta = K_2 \sqrt{\left(\frac{K_1 \mu u_f}{g (\rho - \rho')} \right)} \qquad \text{(A-11)}$$

with K_2 given by (A-10). In case of an inclined tube, g has to be replaced by g cos χ, where χ denotes the inclination to the vertical. The $(\rho-\rho')$-term has been introduced following Fallah et al. (see Portalski, 1963, for instance). When $u(R_1) = 0$ and $K_2 = 1$, they showed that $K_1 = 12$. When the interfacial shear stress increases, the value for K_1 increases. For $K_2 = 1$ Kapitsa derived the value 2.4 for K_2. According to the above treatment, K_2 is given by (A-12) and $K_1 = 3$. The value of K_1 depends on the concentration

of surface-active agents, which tend to suppress rippling. For a higher concentration K_1 is larger. In the case of turbulent films ($R_e > 300$) without interfacial shear stress, Kapitsa's results apply better than Nusselt's (see Portalski, 1963).

LITERATURE AND REFERENCES

Akagawa, K. and Sakaguchi, T.
Fluctuations at void ratio in two-phase flow.
Bulletin Japan. Soc. of Mechan. Engin., 9, page 104, 1966.

Analytis, G.Th. and Lübbesmeyer, D.
Two-phase flow velocity measurements in the upper part of a BWR: the importance of multi-dimensional effects for their interpretation.
ANS reprint. Proceedings of Nuclear Thermal Hydraulics, Winter meeting, 1983.

Banerjee, S. and Chan, A.M.C.
Separated flow models - I. Analysis of the averaged and local instantaneous formulations.
Int. J. Multiphase Flow, Vol 6, page 1, 1980.

Benjamin, T.B.
Instability of periodic wavetrains in nonlinear dispersive systems.
Proc. Roy. Soc. A, 299, page 59, 1967.

Bergles, A.E. and Suo, M.
Investigation of boiling water flow regimes at high pressure.
Proc. of 1966 Heat Transfer & Fluid Mech. Inst., Stanford Univ.Press, 1966.

Bryce, W.M.
A new flow-dependent slip correlation, which gives hyperbolic steam-water flow equations.
European Two-Phase Flow Group Meeting, Grenoble 1977.

Collins, R.; De Moraes, F.F.; Davidson, J.F., and Harrison, D.
The motion of a large gas bubble rising through liquid flowing in a tube.
J. Fluid Mech., 89, 497, 1978.

Davey, A. and Stewartson, K.
On three-dimensional packets of surface waves.
Proc. R. Soc. A, 338, page 101, 1974.

Feir, J.E.
Discussion : some results from wave pulse experiments.
Proc. Roy. Soc. A, 299, page 54, 1967.

Fernandes, R.C.
Experimental an theoretical studies of isothermal upward gas-liquid flows in vertical tubes.
Ph. D. Thesis, Chemical Engineering, Univ. of Houston, 1981.

Filla, M.; Davidson, J.F.; Bates, J.F. and Eccles, M.A.
Gas phase controlled mass transfer from a bubble.
Chem. Engng. Sci., 31, page 359, 1976.

Geld, C.W.M. van der
Flow regime recognition at elevated pressures.
European Two Phase Flow Group Meeting, Rome 1984.
Eindhoven Univ. of Technology, report WOP-WET 84.009.

Haberstroh, R.D. and Griffith, P.
The transition from the annular to the slug flow regime in two-phase flow.
Atomic Energy Commission; DSR No. 5003, Massachusetts Institute of Technology, 1969.

Hetsroni, G.
Handbook of multiphase systems.
McGraw-Hill Book Company, 1982.

Ishii, M.
Thermo-fluid dynamic theory of two-phase flow.
Eyrolles, Paris, 1975.

Jones, O.C.Jr. and Zuber, N.
The interrelation between void fraction fluctuations and flow patterns in two-phase flow.
Int. J. Multiphase Flow, Vol. 2, page 273, 1975.

Kordyban, E. and Ranov, T.
Mechanism of slug formation in horizontal two-phase flow.
J. of Basic Engineering, page 857, 1970.

Lighthill, J.
Waves in fluids.
Cambridge University Press, 1978.

Longuet-Higgins, M.S.
Integral properties of periodic gravity waves of finite amplitude.
Proc. Roy. Soc. A, 342, page 157, 1975.

Luke, J.C.
A variational principle for a fluid with a free surface.
J. Fluid Mech. 27, page 395, 1967.

Moisis, R.
The transition from slug to homogeneous two-phase flows.
Trans. of the A.S.M.E., J. of Heat transfer, page 366, 1963.

Moisis, R. and Griffith, P.
Entrance effects in a two-phase slug flow.
Trans. of the A.S.M.E., J. of Heat transfer, 1962.

Nicklin, D. and Davidson, J.
The onset of instability in two-phase slug flow.
Proc. of symp. on Two-Phase Flow, paper 4, Inst. Mech. Engineering London, 1962.

Portalski, S.
Studies of falling liquid film flow.
Chemical Engineering Science, Vol. 18, page 787, Pergamon Press, Oxford, 1963.

Saito, T.
Multi-fluid modelling of two-phase flow and heat transfer : application to CHF prediction for BWR conditions.
Ph.D. Thesis, Nuclear Engineering, Univ. of Wisconsin, 1977.

Stewart, P.S.B., and Davidson, J.F.
Slug flow in fluidised beds.
Powder Techn., 1, 61, 1967.

Taitel, Y.; Bornea, D. and Dukler, A.
Modelling flow pattern transitions for steady upward gas-liquid flow in vertical tubes.
A.I.Ch.E. J., Vol 26, no 3, page 345, 1980.

Whitham, G.B.
Linear and nonlinear waves.
Wiley & Sons, 1974.

NOMENCLATURE

List of symbols

Roman letters

a	parameter defined by (54)	
	$-\varrho g/2\pi$ in appendix	kg/s^2m^2
A	pseudo-amplitude, (8)	m
A'	parameter connected with pseudo-amplitude A, (31)	m/s
A"	parameter connected with pseudo-amplitude A, (35)	m^2/s
b	parameter defined by (55)	
c	wave velocity, see figure 1 (laboratory frame)	m/s
d	parameter defined by (56)	
D	inside diameter of the tube	m
f	parameter defined by (37)	-
$\bar{f}$	$\frac{d}{d\bar{k}} \mid_{k_o} f$	m
F	amplitude shearing parameter, (8)	-
F"	amplitude shearing parameter, (35)	-
$\bar{F}$	$\frac{d}{d\bar{k}} \mid_{k_o} F$	m
g	acceleration of gravity at earth's surface	m/s^2
h	thickness of the liquid film	m
h'	radius of the gas/vapor core in a Taylor bubble	m
i	$\sqrt{(-1)}$	
I	modified Bessel functions	
k	wave number $2\pi/\lambda$	m^{-1}
k_o	wave number determined as described in 1.2	m^{-1}
K_1	defined by (A-13) in the appendix	-
K_2	$\sqrt{(D-h)/(D-2h)}$	-
l_E	entry length	m
L_p	length of a plug	m
$\dot{m}$	density of total mass flow rate	kg/m^2s
p	pressure	N/m^2
$\underline{q}'$	velocity vector of the gas/vapor phase	m/s
$\hat{r}$	unit vector defined in figure 1	m

R	radius of the tube	m
t	time	s
T	temperature	^{o}C
u	total velocity	m/s
$\bar{u}$	undisturbed velocity	m/s
$\hat{u}$	disturbance velocity	m/s
u_f	film velocity magnitude (positive when downward) (upward ≡ parallel to the gravity vector)	m/s
U	mean velocity magnitude (positive when upward)	m/s
v	mean velocity magnitude (positive when upward)	m/s
v_r	local velocity component in radial direction	m/s
v_z	local velocity component in axial direction	m/s
$\hat{x}$	unit vector defined in figure 1	m
$\hat{y}$	unit vector defined in figure 1	m
z	axial coördinate, see figure 1	m

Greek letters

α	local phase (section 1.1.2)	-
γ	$(1/D)\ K_2 \sqrt{\ \{\ K_1\eta/g(\varrho-\varrho')\ \}}$	$\sqrt{(s/m)}$
δ	thickness of the liquid film	m
ε	void fraction	-
ζ	Lagrangian density	kg/s^2
η	local deviation of the interface	m
η'	$\frac{\partial}{\partial z}\eta$	-
η''	$\partial^2\eta/\partial z^2$	m^{-1}
θ	$h'-\eta = R-h-\eta$	m
λ	wavelength	m
λ_+	parameter defined by (46)	m^{-1}
λ_-	parameter defined by (46)	m^{-1}
μ	viscosity	kg/m.s
ν	kinematic viscosity	m^2/s
ϱ	mass density	kg/m^3
σ	surface tension	N/m
ξ	parameter defined by (66)	-

φ	velocity potential	m^2/s
	δ/R in the appendix	-
$\bar{\varphi}$	unperturbed velocity potential	m^2/s
ψ	stream function	m^2/s
$\bar{\psi}$	unperturbed stream function	m^2/s
$\hat{\psi}$	perturbation stream function	m^2/s
ω	vorticity (30)	$(ms)^{-1}$
	phase flow rate (section 1)	s^{-1}
ω_o	$\sqrt{(\sigma k^3 \tanh(kh)/\varrho)}$ (section 1.1.2)	s^{-1}

List of subscripts

c	center of the tube
E	entry region
f	film
G	gas-vapor
L	liquid
lim	limiting (section 2.4.3)
max	maximum (section 2.4.3)
o	corresponding to the most dominant wave number
p	plug
r	in the r-direction
s	superficial
SL	slug
sat	saturation
x	in the x-direction
y	in the y-direction
z	in the z-direction

Superscript

hyphen (') denotes the gas/vapor phase, mostly in the core of a Taylor bubble, if there is a choice between liquid and gas/vapor. E.g. : u'_s = superficial gas/vapor velocity ; h' = radius of the gas/vapor core ; but : $\eta' = \frac{\partial}{\partial z}\eta$.

$\hat{x}$	unit vector in x-direction

Acronyms

FACT	defined by (64a)
Im	imaginary part
LHS	left-hand side
MKS	International system of standard units
O(a)	order of a
P-C	Plug-Churn (section 1)
R_e	Reynolds number Uh/ν or U'h'/ν'
RHS	right-hand side
$\|s\|$	absolute norm of s, $\sqrt{\sum_i s_i^2}$
$((j))$	defined by (10) in section 2.1.2 $(j = 1,2,3\ldots,9)$
$((\bar{j}))$	$\frac{d}{d\bar{k}} \mid_{k_o} ((j))$ $(j = 1,2,3\ldots,9)$
{{0}}	defined by (60)
{{1}}	defined by (53)
{{2}}	defined by (53)
{{3}}	defined by (62)
{{4}}	defined by (63)
{{9}}	defined by (61)
$\{\{\bar{j}\}\}$	$\frac{d}{d\bar{k}} \mid_{k_o} \{\{j\}\}$ $(j = 1,2,3,4 \text{ or } 9)$
√{ag}	square root of ag